hydrology

MDPI

Article

The Effects of Input Scale and Metric on Groundwater Level Forecasting with Deep Learning

Halima Hilal [1], Nourelhouda Karmouda [1], Tarik Bouramtane [1,*], Youssef Hamou-Ali [1], Ismail Mohsine [1], Houssne Bouimouass [2], Hassan Mosaid [2], Mounia Tahiri [1], Nadia Kassou [1], Ilias Kacimi [1] and Marc Leblanc [3]

[1] Geosciences, Water and Environment Laboratory, Faculty of Sciences, Mohammed V University in Rabat, Avenue Ibn Batouta, Rabat 10104, Morocco; halima.hilal@um5r.ac.ma (H.H.)
[2] CRSA, Center for Remote Sensing Applications, Mohammed VI Polytechnic University, Ben Guerir, Green City 43150, Morocco
[3] Hydrogeology Laboratory, UMR EMMAH, Avignon University, 84916 Avignon, France
* Correspondence: t.bouramtane@um5r.ac.ma; Tel.: +212-603445240

Abstract

The Normalized Difference Vegetation Index (NDVI) is widely used as an indicator of irrigation activity in arid and semi-arid agricultural regions. This study evaluates how NDVI extraction scale and statistical metric influence groundwater level prediction accuracy in the irrigated Tadla Plain, MoroccoA total of 96 Long Short-Term Memory (LSTM) models were developed by combining six NDVI extraction scales, from the well pixel to 20,000 m buffers, and four statistical metrics: mean, median, maximum, and minimum. Results demonstrate that extraction scale is a critical factor controlling model performance. Across the four monitored wells, larger buffers ($\geq$2500 m) generally outperformed smaller ones ($\leq$1000 m), with the optimal scale occurring at 15,000 m for three wells, while one well achieved its best performance at the 1000 m scale. The best models achieved RMSE values between 0.09 and 0.625 m and R^2 values ranging from 0.94 to 0.997. Maximum NDVI provided the highest predictive accuracy for three wells, whereas minimum NDVI performed best for one well. Statistical analyses further confirmed that extraction scale generally exerts a stronger influence on prediction performance than the choice of NDVI metric. Spatial validation revealed that irrigated areas more than doubled between 2001 and 2017, and model performance improved as NDVI captured this broader irrigation footprint. These findings suggest that groundwater level variations in the Tadla Plain are more strongly associated with NDVI signals extracted at broader spatial scales than with strictly local vegetation conditions around individual wells, highlighting the importance of optimizing both NDVI extraction scale and metric for groundwater forecasting in irrigated semi-arid regions.

Keywords: groundwater modeling; LSTM neural network; NDVI spatial scale; vegetation index metrics; semi-arid hydrology; remote sensing

Check for updates

Academic Editor: Emanuele Barca

Received: 6 May 2026
Revised: 24 June 2026
Accepted: 1 July 2026
Published: 17 July 2026

Copyright: © 2026 by the authors. Licensee MDPI, Basel, Switzerland. This article is an open access article distributed under the terms and conditions of the Creative Commons Attribution (CC BY) license.

1. Introduction

Groundwater depletion threatens agricultural sustainability across arid and semi-arid regions where irrigation depends heavily on aquifer resources increasingly stressed by climate variability and overexploitation [1–3]. In Morocco, irrigated agriculture's economic importance intensifies this pressure, particularly during the unprecedented eight-year drought beginning in late 2017 that has driven critical aquifer declines through reduced recharge and intensified pumping.

The Normalized Difference Vegetation Index (NDVI), derived from red and near-infrared reflectance [4–6], has emerged as a valuable proxy for groundwater-dependent irrigation. Higher NDVI values indicate active crop growth and water availability [7], particularly where vegetation depends on groundwater use [8,9]. Recent studies demonstrate NDVI's effectiveness as input for machine learning models, especially Long Short-Term Memory (LSTM) networks, in forecasting groundwater levels under irrigation pressure [10–13]. Feature importance analysis revealed NDVI as the dominant variable for irrigated wells [12], with strong correlations to groundwater levels in floodplain aquifers [14,15] and successful application in GRACE downscaling from 100 km to 1 km resolution [16].

Despite NDVI's proven utility, two critical methodological gaps persist. First, the influence of NDVI extraction buffer size on vegetation–groundwater relationships remains largely unexplored, though buffer size significantly affects observed associations with environmental variables [17–20]. In heterogeneous agricultural landscapes, varying buffer sizes alter perceived vegetation patterns [21–23], potentially leading to spatial misclassification. Second, the choice of statistical metric, mean, median, maximum, minimum, for summarizing NDVI within buffers significantly affects irrigated area detection [24–29], yet its impact on groundwater monitoring remains unassessed.

This study is built on the conceptual assumption that, in intensively irrigated semi-arid systems, groundwater level fluctuations are partly controlled by spatially distributed irrigation activity, which can be indirectly captured through vegetation dynamics [2,6,22]. NDVI is therefore considered here as a remote sensing proxy for irrigation intensity, while the extraction scale and statistical metric determine how this vegetation signal is spatially represented around observation wells [8,17,19,21]. Based on this framework, we systematically investigate how NDVI extraction scale and metric selection influence groundwater level prediction using LSTM neural networks [10,12,13]. NDVI time series were extracted using four statistical metrics across seven spatial scales, from the well pixel to 20,000 m buffers, and used as inputs to forecast groundwater levels at four monitoring wells in the Tadla irrigated plain, Morocco. This approach allows us to assess whether groundwater dynamics are better explained by local vegetation conditions near the well or by broader irrigation patterns acting at the regional scale.

2. Materials and Methods

2.1. Study Area

The Tadla Plain in Morocco's Oum Er Rbia basin provides ideal conditions for assessing NDVI extraction scale impacts on groundwater prediction accuracy (Figure 1). Spanning over 320,000 hectares with more than 124,000 hectares irrigated [30], the region experiences intense groundwater exploitation driven by recurrent droughts, particularly the prolonged dry period from late 2017 lasting over seven years. The plain is one of Morocco's most intensely exploited aquifers despite severe water stress [31,32].

The region exhibits relatively uniform topography at 400 m average elevation with gentle westward slopes, 1–3‰ [33]. Stretching 125 km by 40 km, it is hydrogeologically divided by the Oum Er-Rbia River into Beni Amir, north, and Beni Moussa, south, aquifers. The arid to semi-arid climate receives 300–750 mm annual precipitation, with extremely hot summers intensified by dry Chergui winds [34].

The Tadla plain in central Morocco is a broad, low-relief alluvial basin south of the Moroccan Meseta and bounded to the south and east by the Middle and High Atlas. The plain is crossed from east to west by the Oued Oum Er-Rbia, which separates the irrigated land into two large schemes managed by the Office Régional de Mise en Valeur Agricole du Tadla: the Béni Amir perimeter on the right (northern) bank and the more

extensive Béni Moussa perimeter on the left (southern) bank. The climate is arid to semi-arid, with mean annual rainfall of about 300 mm and a long, hot dry season, so that cultivation depends almost entirely on irrigation. Surface water delivered by gravity predominates, supplemented by groundwater pumping and, increasingly, localized drip and pivot systems; land use is dominated by irrigated field and tree crops—cereals, sugar beet, fodder and alfalfa, citrus and olive, and market gardening [35–44].

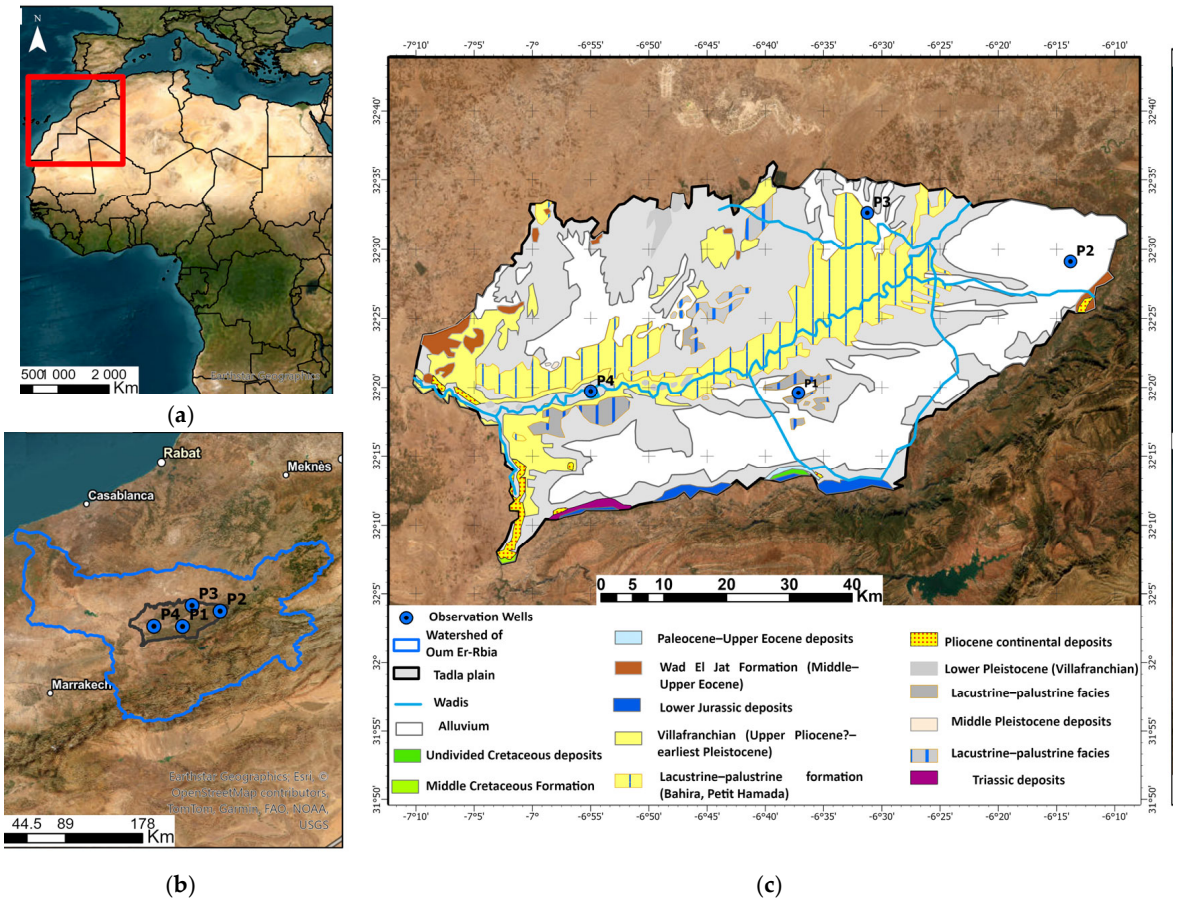

Figure 1. Location Maps. (**a**) Location of the study area in North Africa and in Morocco, respectively; (**b**) location of the observation wells within the Oum Er Rbia basin; and (**c**) location of the observation wells within the irrigated area of the Tadla plain with the geology.

Groundwater occurs in a multilayer aquifer system. From top to bottom this comprises: i. the Mio–Plio–Quaternary unconfined complex (the unconfined Béni Amir and Béni Moussa water tables within the alluvial fill); ii. a semi-confined Eocene aquifer that crops out at the basin margins and becomes captive beneath the plain, iii. the Senonian, and iv a deep, confined to karstic Turonian limestone aquifer, underlain by a weathered Primary basement. Geologically, the Mio–Plio–Quaternary formations comprise alternating conglomerates, sandstones, marls, and lacustrine deposits creating complex groundwater flow patterns where lithology strongly influences permeability distribution [34,35]. Recharge of this aquifer occurs through direct infiltration and irrigation return flows, with additional surface water from Bin El Ouidane Dam, approximately 100 km upstream. The water table of the Mio–Plio–Quaternary aquifer typically lies 5–6 m beneath hardened limestone crust, flowing north–northwest with seasonal fluctuations tied to irrigation cycles [36].

Groundwater occurs in a multilayer aquifer system. From top to bottom this comprises the Mio–Plio–Quaternary phreatic complex—the unconfined Béni Amir and Béni Moussa nappes within the alluvial fill—a semi-confined Eocene aquifer that crops out

at the basin margins and becomes captive beneath the plain, the Senonian, and a deep, confined to karstic Turonian limestone aquifer, underlain by a weathered Primary basement. The four boreholes were sited to monitor three of these units on both banks of the Oum Er-Rbia.

2.2. Observed Groundwater Level Records

The four monitoring boreholes lie in the Tadla plain. The four observation wells were selected from the available monitoring network based on the length and completeness of their monthly groundwater level records within the Tadla irrigated perimeter. They were also chosen because they are located in irrigated areas and represent different hydrogeological contexts within the Tadla plain, including the Beni Moussa, Beni Amir and deep Tadla aquifer systems. This selection provides suitable temporal continuity for LSTM modeling while capturing part of the hydrogeological heterogeneity of the region. Nevertheless, the limited number of wells remains a constraint and is considered when interpreting the spatial generalization of the results.

Monitoring bore characteristics are compiled in Table 1. On the left (southern) bank, P1 (IRE 420-36) taps the unconfined Plio–Quaternary aquifer in the western Béni Moussa sector, east of Souk Sebt Oulad Nemma, at about 429 m. Some 40 km to the east–northeast, near the eastern head of the plain, P2 (IRE 1203-36) monitors the confined Turonian aquifer in the Béni Moussa-Est sector, about 13 km south–southeast of Kasba Tadla and close to the Atlas-fed eastern margin of the perimeter. On the right (northern) bank, P3 (IRE 1525-37) also samples the confined Turonian, in the Béni Amir perimeter north-east of Fkih Ben Salah toward El Borouj, at about 470 m. At the opposite, downstream end of the plain, P4 (IRE 4887-36) taps the semi-confined Eocene aquifer at the western margin of Béni Moussa, west of Oulad Ayad, at 374 m—the lowest of the four sites, consistent with the westward fall of the plain. The network thus spans roughly 65 km across the basin, from its eastern apex (P2) to its western outlet (P4), and brackets the three principal aquifers targeted for monitoring.

The soils at the sites belong to the brown, broadly isohumic subtropical soils that dominate the Tadla perimeter, but their parent materials differ between the two banks. Béni Amir soils (P3) developed on calcareous brown silts and tufa derived from the Phosphate Plateau and Cretaceous marls, whereas the Béni Moussa soils (P1, P2 and P4) formed on more clayey, less calcareous and locally rubefied alluvium of Atlasic origin. Less-evolved erosional and calcimagnesic soils fringe the Oued Oum Er-Rbia and the perimeter margins. Secondary salinisation is a recognized phenomenon in the area and most pronounced in Béni Amir and western Béni Moussa [37].

Well P1 has a mean groundwater level of 413.89 m, with a standard deviation of 2.62 m and a range of 408.14–418.82 m. Well P2 shows the highest variability, with a mean of 346.07 m, a standard deviation of 4.75 m, and a range of 335.02–355.99 m. Well P3 exhibits a mean groundwater level of 417.39 m, with a standard deviation of 1.5 m and a range of 413.4–419.94 m. Well P4 has a mean groundwater level of 436.12 m, with a standard deviation of 4.21 m and a range of 426.03–443.05 m (Table 2). In Figure 2a, the density axis represents the kernel density estimate of groundwater level values, indicating where observations are more concentrated within the groundwater level range for each well. Time series were split into training (February 2009–November 2017, 90%) and validation (December 2017–December 2018, 10%) periods, allowing model evaluation over complete hydrological and cropping cycles (Figure 2b). This consistent partitioning enables direct performance comparison across wells and assessment of spatial heterogeneity in NDVI–groundwater relationships.

Table 1. Characteristics of the four monitoring boreholes, Tadla plain.

	P1/IRE 420-36	P2/IRE 1203-36	P3/IRE 1525-37	P4/IRE 4887-36
Aquifer	Plio–Quaternary alluvial aquifer system	Turonien	Turonien	Eocene
Aquifer type	unconfined	confined	confined	semi-confined
X (lambert)	385,071	421,855	394,609	357,104
Y (lambert)	193,072	210,269	217,046	193,664
Z (m a.s.l.)	429	≈500 (approx.) [1]	470	374
Latitude (WGS 84)	32.326851° N	32.485216° N	32.544044° N	32.328883° N
Longitude (WGS 84)	6.619345° W	6.230052° W	6.520763° W	6.916499° W
Bore usage	monitoring	monitoring	monitoring	monitoring
Sub-perimeter/location	Béni Moussa	Eastern Tadla	Béni Amir	Béni Moussa, western margin of the perimeter
Land use [1]	Irrigated agriculture–Béni Moussa perimeter (cereals, sugar beet, fodder/alfalfa, citrus & olive, market gardening)	Irrigated agriculture–Béni Moussa-Est (cereals, sugar beet, fodder, olive/citrus).	Irrigated agriculture–Béni Amir perimeter (cereals, sugar beet, fodder, orchards).	Irrigated cropland at the western perimeter margin; grades into rainfed cereal
Soil type [1]	Brown subtropical isohumic soils on Atlasic alluvium (Béni Moussa)–more clayey, less calcareous, locally rubefied; vertisols/red Mediterranean soils locally	Béni Moussa isohumic soils on Atlasic alluvium (more clayey, less calcareous, locally rubefied); calcimagnesic/less-evolved soils possible toward the eastern piedmont	Brown isohumic/calcimagnesic soils on calcareous brown silts & tufa	Béni Moussa isohumic soils grading, toward the margin/Oued Oum Er-Rbia, to less-evolved erosion and calcimagnesic soils
Distance to closest irrigated area [2]	≈0 m (within Béni Moussa irrigated perimeter)	≈0 m (within Béni Moussa-Est irrigated land).	≈500 m (within Béni Amir irrigated perimeter)	≈0 m

[1]. Land use was characterized by the regional setting [38–40]. Soils were characterized by the SCET-Maroc 1:100,000 soil survey [37–40]. [2]. Distances to irrigated land determined by photointerpretation of recent high resolution satellite imagery (Sentinel 2, May 2026). The irrigated perimeters are visually unmistakable against the semi-arid surroundings in high resolution imagery on GoogleEarth.

Table 2. Descriptive statistics of groundwater levels.

Well	Record (n)	Mean (m)	Std Dev (m)	Minimum (m)	Maximum (m)	Average Seasonal Amplitude (m) (Annual/Detrended)	Long-Term Trend, Theil Sen (m)
P1 (IRE 420_36)	2009–2018 (n = 119)	413.89	2.62	408.14	418.82	4.4 m/2.4 m	−0.72 m/yr
P2 (IRE 1203_36)	2007–2018 (n = 128)	547.21	1.69	541.57	549.98	2.7 m/2.2 m	−0.32 m/yr
P3 (IRE 1525_37)	2008–2018 (n = 129)	436.12	4.21	426.03	443.05	5.4 m/4.4 m	−1.07 m/yr
P4 (IRE 4887_36)	2008–2017 (n = 113)	346.07	4.75	335.02	355.99	9.6 m/8.7 m	−0.51 m/yr

Over their roughly decade-long records (2008–2018), all four monitored aquifers show statistically significant declines in groundwater level (Mann–Kendall, $p < 0.01$). The Theil–Sen rates range from −0.32 m/yr in the Turonian at P2 and −0.51 m/yr in the Eocene at P4, through −0.72 m/yr in the phreatic Plio–Quaternary nappe at P1, to −1.07 m/yr in the Turonian at P3; losses of roughly 4 to 11 m of head over the period (Table 2). The average

seasonal amplitude widens with depth and confinement: it is largest in the low-storage Eocene at P4 (about 9 m) and the Turonian at P3 (about 5 m), and smallest in the high-storage phreatic nappe at P1 and the Turonian at P2 (about 2 m), with water levels highest in winter (December–February, after recharge) and lowest in late summer (July–September, at peak irrigation pumping). The Béni Moussa phreatic nappe (P1), which rose historically under irrigation return flow, is now itself in decline, consistent with a shift toward net depletion under drought and intensified abstraction.

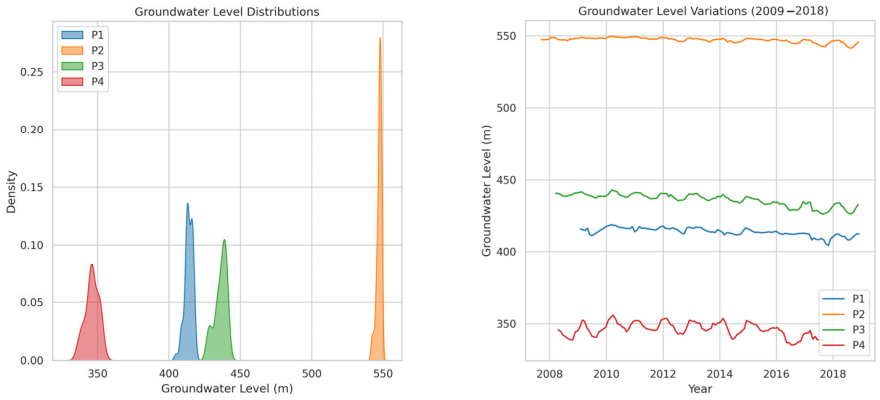

Figure 2. Groundwater level distributions and temporal variations for the four monitoring wells. (**a**) Kernel density distributions of groundwater level values, where the density axis represents the relative concentration of observations within each groundwater level range; (**b**) groundwater level variations over the period 2009–2018, expressed in meters.

2.3. Normalized Difference Vegetation Index (NDVI)

Monthly NDVI values were extracted from MOD13Q1 Version 6 Terra MODIS sensor data at 250 m spatial resolution and 16-day temporal frequency. NDVI time series were generated using circular buffers around each well following established methodologies [17,19]. Six buffer radii were defined: 500, 1000, 2500, 10,000, 15,000, and 20,000 m (Figure 3). Additionally, single-pixel extraction at well locations, termed "0 m", provided direct NDVI values without buffering.

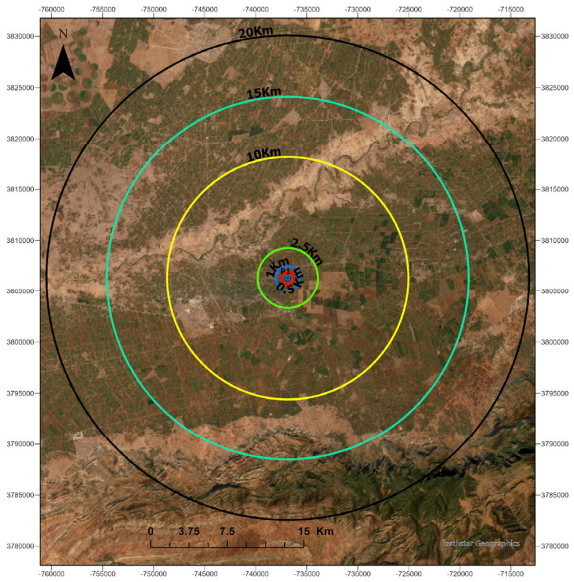

Figure 3. NDVI Extraction Scales Map. Spatial map showing the six NDVI extraction buffer scales (500 m, 1000 m, 2500 m, 10,000 m, 15,000 m, 20,000 m) as concentric circles around a well location.

For each extraction scale, four NDVI metrics, namely mean, median, maximum, and minimum, were computed on a monthly basis. Figure 4 illustrates the temporal NDVI variations for well P1 across the seven extraction scales, 0 m, 500 m, 1000 m, 2500 m, 10,000 m, 15,000 m, and 20,000 m, during the 2009–2018 period. The corresponding NDVI time-series figures for wells P2, P3, and P4 are provided in the Supplementary Material as Figures S1–S3, respectively. Mean NDVI shows moderate values with lower variability; median NDVI provides slightly higher and more robust values resistant to extremes; maximum NDVI consistently captures peak vegetation vigor; and minimum NDVI reflects the driest or non-irrigated areas within the buffers.

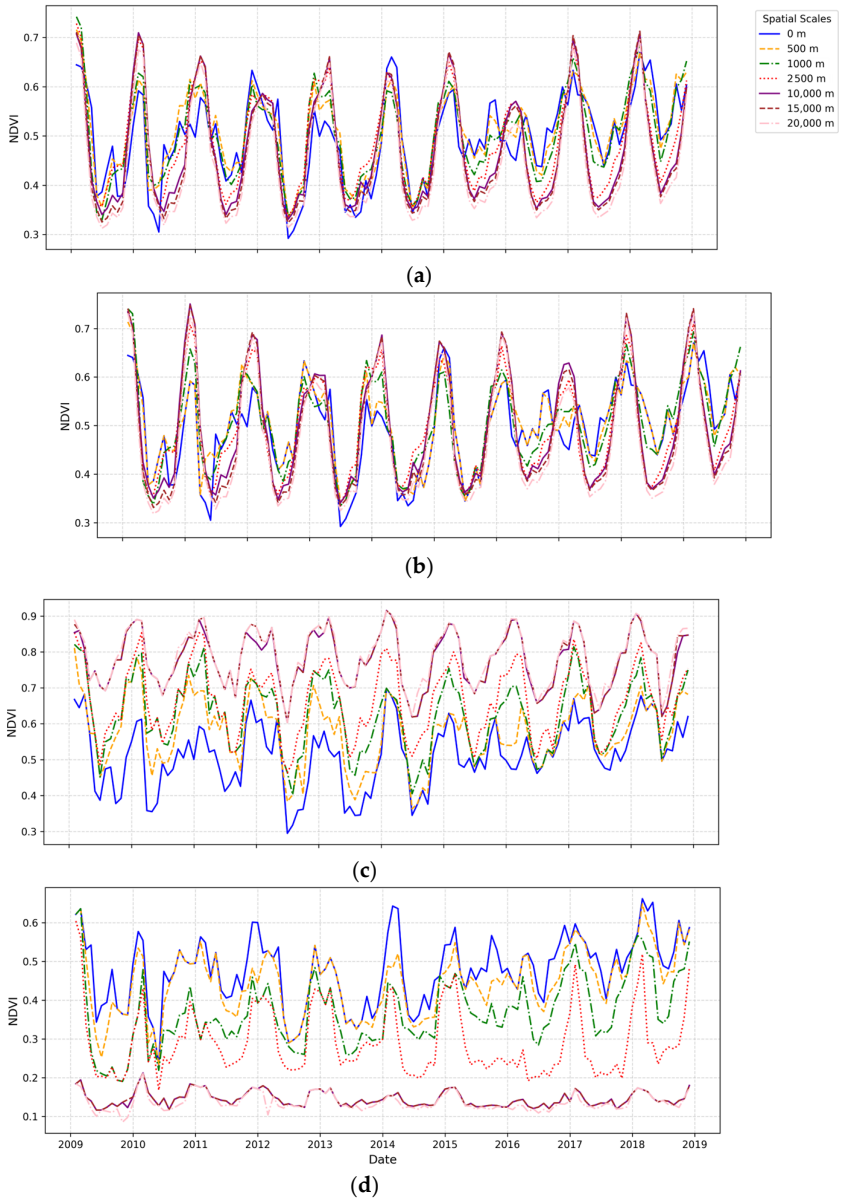

Figure 4. Temporal NDVI variations for well P1 across the different extraction scales. Monthly NDVI time series for the period 2009–2018 are shown for the seven extraction scales: 0 m, 500 m, 1000 m, 2500 m, 10,000 m, 15,000 m, and 20,000 m. Panels show: (**a**) mean NDVI; (**b**) median NDVI; (**c**) maximum NDVI; (**d**) minimum NDVI.

This approach produced 96 distinct NDVI time series, corresponding to 24 combinations per well across four wells. Although the largest buffers extend beyond irrigated

boundaries, NDVI extraction was restricted to the Tadla aquifer geological limits, ensuring that only hydraulically connected vegetation signals were captured.

2.4. Long Short-Term Memory (LSTM) Model

Long Short-Term Memory networks were selected for their proven ability to capture temporal fluctuations and complex dynamics in groundwater time series. Unlike feedforward networks, LSTM architecture processes sequential data effectively through memory cells and gated mechanisms retaining relevant patterns over long intervals, which is essential for understanding delayed or cumulative hydrogeological effects.

Traditional Recurrent Neural Networks face vanishing gradient problems during backpropagation through time, limiting long sequence learning [45–47]. LSTM overcomes this through specialized architecture including Constant Error Carousel memory cells and three gate types, input, forget, and output gates, regulating information flow while maintaining stable gradient calculations [48]. The information is processed by a sequential calculation using the following equations iteratively along the time series:

$$i_t = \sigma(w_i x_t + U_i h_{t-1} + b_i) \quad (1)$$

$$f_t = \sigma(w_f x_t + U_f h_{t-1} + b_f) \quad (2)$$

$$o_t = \sigma(w_o x_t + U_o h_{t-1} + b_o) \quad (3)$$

$$\overline{C} = Tanh(x_t + U_c h_{t-1} + b_c) \quad (4)$$

$$C_t = f_t \otimes C_{t-1} + i_t \otimes C_t \quad (5)$$

$$h_t = o_t \otimes Tanh\,(C_t) \quad (6)$$

In these equations, wi, wf, and wo refer to the input weight matrices associated with the input, forget, and output gates, respectively. Likewise, Ui, Uf, and Uo correspond to the recurrent weight matrices linking the previous hidden state to these three gates. The terms bi, bf, and bo denote the bias vectors of the input, forget, and output gates. The symbol σ\sigmaσ represents the element-wise logistic sigmoid activation function. At time step t, it, ft, ot, and Ct represent the input gate, forget gate, output gate, and cell state, respectively. These vectors have the same dimensionality as the hidden output vector ht. The operator ⊗ indicates element-wise multiplication between vectors [48].

The LSTM architecture comprises two stacked layers. The first returns sequences, preserving temporal patterns for the second layer, which condenses sequences into compact representations. Dropout layers after each LSTM layer prevent overfitting by randomly deactivating neurons during training. A final Dense layer with a single neuron generates groundwater level predictions. The Adam optimizer with mean squared error loss function adjusts weights. Two-layer depth generally suffices for capturing vegetation–groundwater interactions [11,48].

In total, 96 LSTM models were developed, corresponding to 24 model configurations for each well. Each configuration was defined by a unique NDVI time series obtained from the combination of one extraction scale and one statistical metric. For each model, a single NDVI time series was used as the input variable, while the corresponding groundwater level time series of the same well was used as the output variable. This design allowed the effect of NDVI extraction scale and metric selection to be evaluated independently and consistently across all wells.

To optimize model performance, hyperparameter tuning was performed separately for each LSTM model using the GridSearchCV approach. Grid search is a systematic optimization method that tests all predefined combinations within a selected hyperparameter space and identifies the configuration that provides the best model performance [49,50]. In this

study, the tuned hyperparameters included the number of neurons, batch size, learning rate, dropout rate, and number of epochs. The dropout rate was used to reduce overfitting by randomly deactivating neurons during training, while the batch size controlled the number of samples processed before updating the model weights. The number of epochs defined the number of complete passes through the training dataset. Applying GridSearchCV independently to each model ensured that every NDVI scale–metric–well combination was evaluated using its optimal LSTM configuration.

Three performance metrics evaluated model comparison: Root Mean Squared Error, Mean Absolute Error, and coefficient of determination, R^2 [12,16]. RMSE and MAE measure accuracy by quantifying average error magnitude, with RMSE more sensitive to large deviations. R^2 assesses how well predictions reproduce observed variability. In addition to these numerical indicators, violin plots and Taylor diagrams were used to facilitate graphical model comparison. Violin plots display the distribution of model performance values across NDVI extraction scales and metrics, allowing visual comparison of variability and dispersion. Taylor diagrams provide a graphical comparison of model performance by jointly representing the standard deviation and correlation coefficient, which enables a more direct evaluation of the relative performance of the different models.

2.5. Statistical Validation Method

The Kruskal–Wallis H-test, a rank-based non-parametric test for comparing multiple groups without assuming normality [51–55], evaluated NDVI buffer size and metric effects on each performance indicator separately. Tests were conducted on 96 LSTM model results, each trained using unique buffer size, NDVI metric, and well combinations. For each indicator, models were grouped by extraction scale or metric, assessing whether observed performance differences across groups were statistically significant. This identified meaningful variations attributable to spatial extent or descriptor choice. *p*-values were interpreted at 95% confidence, $\alpha = 0.05$, with tests performed both per well and pooled to assess study area consistency.

2.6. Spatial Validation Method

Spatial validation assessed whether NDVI-derived irrigation signals effectively capture irrigated vegetation dynamics and correspond to areas where irrigation likely influences groundwater. Temporal NDVI analysis over the entire Tadla plain, 2000–2020, identified four dates with the lowest summer average NDVI: July 2001, July 2005, July 2010, and July 2017, corresponding to major Moroccan drought episodes when natural vegetation is sparse unless irrigation-supported [8,56].

Irrigated areas were delineated using an NDVI threshold of 0.45, following previous applications of MODIS NDVI for irrigation mapping in semi-arid environments [8,56]. This threshold is particularly relevant during drought periods, when natural vegetation and rainfed crops are generally affected by water stress and therefore exhibit reduced NDVI values. Under these conditions, pixels with NDVI values exceeding 0.45 are more likely to correspond to vegetation maintained by irrigation. Accordingly, NDVI > 0.45 was used as a proxy for active irrigated vegetation. For each buffer scale and selected drought date, the area exceeding this threshold was calculated in km^2. This procedure enabled the quantification of the irrigation footprint within each extraction scale and provided a spatial basis for interpreting the relationship between NDVI-derived irrigation signals and groundwater prediction performance across the four wells.

3. Results

3.1. Effect of NDVI Extraction Scale on Groundwater Level Prediction

Table 3 synthesizes best predictive performance per well, highlighting optimal extraction scale and NDVI metric combinations. Detailed metrics for all 96 models (RMSE, MAE, R^2) over validation periods appear in Supplementary Material (Tables S1, S3, S5 and S7 for P1, P2, P3, P4).

Table 3. Summary of best predictive performance for each well.

Well	Best Scale (m)	Best Metric	RMSE (m)	MAE (m)	R^2
P1	15,000	Maximum	0.090	0.075	0.997
P2	1000	Maximum	0.347	0.254	0.990
P3	15,000	Minimum	0.625	0.465	0.940
P4	15,000	Maximum	0.168	0.142	0.979

Well P1 achieved best accuracy at 15,000 m with maximum NDVI: RMSE 0.09 m, MAE 0.07 m, R^2 0.997. Poorest performance occurred at 0 m with median NDVI: RMSE 0.587 m, MAE 0.516 m, R^2 0.98 (Table S1). Averaged across metrics, larger scales (2500–20,000 m) consistently outperformed smaller ones. Broader scales yielded average RMSE 0.250 m and MAE 0.204 m, while narrower scales (0–1000 m) resulted in significantly higher errors: average RMSE 0.458 m, MAE 0.420 m.

Well P2 showed best performance at 1000 m with maximum NDVI (RMSE 0.347 m, MAE 0.254 m, R^2 0.99), followed by 15,000 m with same metric (RMSE 0.443 m, MAE 0.357 m, R^2 0.968) (Table S3). Averaged across metrics, 1000 m provided best results (average RMSE 0.437 m, MAE 0.340 m), followed by 15,000 m and 20,000 m scales (Table S4). Across all scales, maximum NDVI showed best overall performance (average RMSE 0.452 m, MAE 0.357 m).

Well P3 exhibited optimal performance at 15,000 m with minimum NDVI (RMSE 0.625 m, MAE 0.465 m, R^2 0.940), followed by 20,000 m with same metric (RMSE 0.660 m, MAE 0.436 m, R^2 0.946) (Table S5). Averaged across metrics, 15,000 m and 20,000 m scales outperformed smaller buffers (average RMSE 0.743 m and 0.765 m) (Table S6). Across all scales, minimum NDVI consistently provided best results (average RMSE 0.837 m).

Well P4 achieved highest accuracy at 15,000 m with maximum NDVI (RMSE 0.168 m, MAE 0.142 m, R^2 0.979) (Table S7). Averaged, 15,000 m provided best results across metrics (average RMSE 0.288 m, MAE 0.203 m), followed by 10,000 m (Table S8). While maximum NDVI showed strongest performance at 15,000 m, minimum NDVI achieved best average across all scales (average RMSE 0.893 m).

Performance improvement with larger buffers reflects their capture of wider irrigated land portions influencing regional groundwater, whereas smaller buffers are more sensitive to local NDVI anomalies or noise. However, optimal scale varies: P2 prefers intermediate 1000 m while P1, P3, P4 favor 15,000 m. This heterogeneity likely reflects differences in hydrogeological connectivity, well depth, aquifer properties, and spatial pumping distribution around monitoring points.

Violin plots for the four wells and Taylor diagrams for well P1 (Figures 5 and 6) illustrate the combined effects of NDVI extraction scale and metric selection on model performance. The Taylor diagrams for wells P2, P3, and P4 are provided in the Supplementary Material as Figures S4–S6, respectively, to improve readability. Overall, predictions obtained from larger extraction scales generally reproduce the observed groundwater level distributions more closely, particularly for median and maximum NDVI. This pattern is especially clear for P1, P3, and P4, where larger buffers, mainly between 2500 and 20,000 m, show better agreement with observed distributions and reduced prediction bias.

Smaller buffers, especially 0 and 500 m, tend to produce narrower predicted distributions, with weaker representation of observed variability.

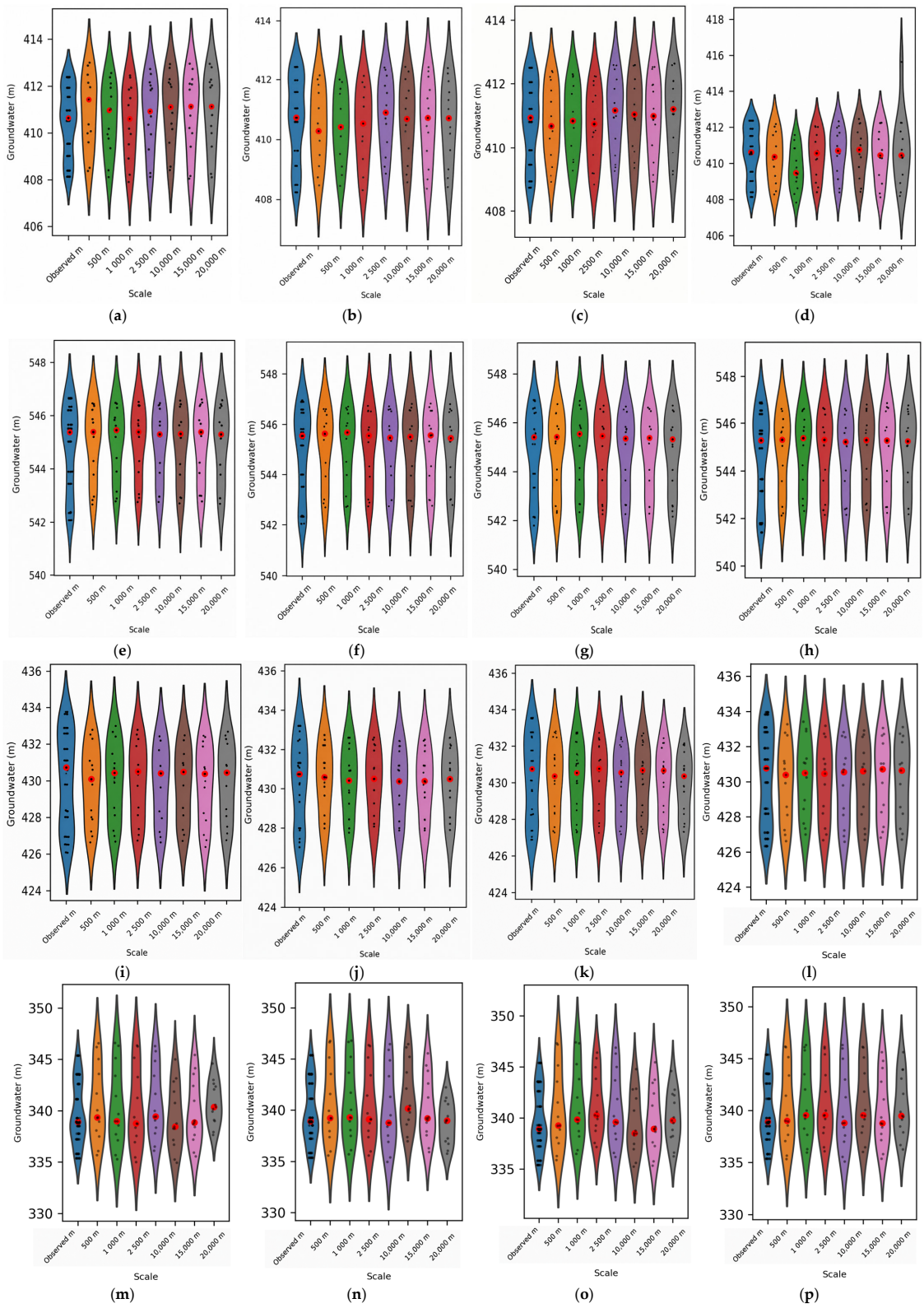

Figure 5. Violin plots comparing observed and predicted groundwater level distributions for wells P1, P2, P3, and P4. Panels show: (**a**–**d**) well P1 using mean, median, maximum, and minimum NDVI, respectively; (**e**–**h**) well P2 using mean, median, maximum, and minimum NDVI, respectively; (**i**–**l**) well P3 using mean, median, maximum, and minimum NDVI, respectively; and (**m**–**p**) well P4 using mean, median, maximum, and minimum NDVI, respectively.

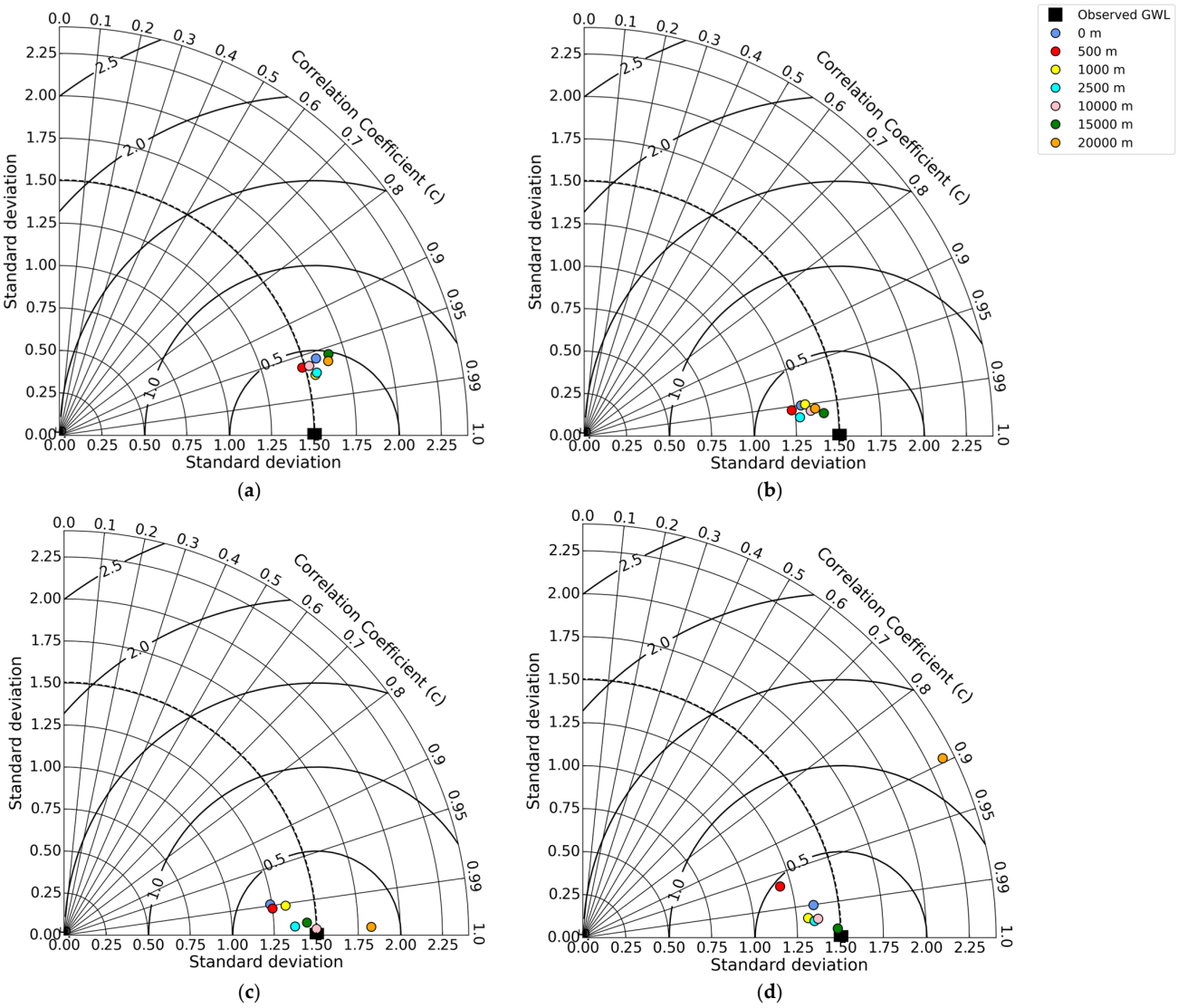

Figure 6. Taylor diagrams showing model performance across NDVI extraction scales for wells P1. The black dot represents the reference point corresponding to the observed groundwater level data. Panels show the results for well P1 using (**a**) mean NDVI, (**b**) median NDVI, (**c**) maximum NDVI, and (**d**) minimum NDVI.

Taylor diagrams further support these results by showing that the best-performing scale–metric combinations generally plot closer to the observed reference point. For P1, shown in Figure 6, the strongest agreement is mostly observed at larger extraction scales, particularly around 15,000 m. Similar graphical analyses for P3 and P4, provided in Figures S5 and S6, also indicate better performance at larger scales, whereas P2, shown in Figure S4, presents its best performance at 1000 m while maintaining good performance at larger scales. These graphical analyses support the quantitative results and highlight that optimal NDVI extraction scale may vary among wells, although broader scales generally provide more stable model performance.

3.2. Influence of NDVI Metrics on Groundwater Level Prediction

LSTM model predictive accuracy varies notably with NDVI metric choice across wells, though specific preferences differ by location. For well P1, maximum NDVI consistently yields best results: RMSE as low as 0.09 m, MAE down to 0.07 m, R^2 between 0.98 and 0.99 across scales. This strong performance indicates maximum NDVI effectively captures

peak vegetation conditions more representative of active irrigation. Median NDVI also performs well, showing stability across scales with RMSE 0.28–0.59 m, MAE 0.22–0.51 m, R^2 reaching 0.99. Its stability explains why median NDVI predictions cluster tightly around observed data in Taylor diagrams, particularly for 2500–15,000 m scales. Mean NDVI exhibits greater variability: RMSE 0.21–0.58 m, MAE 0.18–0.54 m, generally lower R^2 (0.917–0.947), suggesting averaging dilutes strong irrigation signals when mixed with lower NDVI areas.

Minimum NDVI shows the widest error range: RMSE up to 0.82 m, MAE up to 0.73 m. While performing reasonably at intermediate scales (notably 15,000 m), performance degrades at very small (500 m) or large (20,000 m) scales, tending to overestimate extremes and compress observed distribution. Overall, violin plots and Taylor diagrams confirm maximum and median NDVI provide most consistent reliable predictions across scales, remaining closest to reference points in Taylor diagrams, particularly between 2500 and 15,000 m.

For P2, maximum NDVI generally provides strongest performance across most scales, with best results at 1000 m (RMSE 0.347 m, MAE 0.254 m, R^2 0.99) (Table S3). Averaged across scales, maximum NDVI showed best overall performance (average RMSE 0.452 m, MAE 0.357 m), followed by median NDVI (average RMSE 0.475 m) (Table S4). Mean and minimum metrics showed more variable performance.

For well P3, a distinct pattern emerges where minimum NDVI yields best results at larger buffers. At an optimal 15,000 m scale, minimum NDVI achieved RMSE 0.625 m, MAE 0.465 m, R^2 0.940 (Table S5). Averaged across scales, minimum NDVI consistently provided the best results (average RMSE 0.837 m), followed by mean NDVI (average RMSE 0.797 m) (Table S6). This suggests for P3, vegetation stress indicators or sparse coverage may be more informative of groundwater dynamics than peak greenness.

For P4, maximum NDVI provides strongest performance at an optimal 15,000 m scale (RMSE 0.168 m, MAE 0.142 m, R^2 0.979) (Table S7). However, averaged across scales, minimum NDVI achieves best average performance (average RMSE 0.893 m), suggesting while maximum NDVI excels at specific scales, minimum NDVI offers more consistent performance across full buffer range (Table S8).

Variability in optimal metrics across wells highlights site-specific calibration importance. While maximum NDVI generally effectively captures irrigation intensity (wells P1, P2, P4), minimum NDVI success for wells P3, P4 suggests in some locations, vegetation stress or non-irrigated area extent within buffers may provide complementary information about groundwater extraction patterns.

3.3. Kruskal–Wallis Test Results

Kruskal–Wallis tests assessed statistical significance of model performance differences across extraction scales and NDVI metrics for each well individually (Table 4). For well P1, extraction scale significantly affects prediction errors: p-values 0.0205 (RMSE) and 0.0099 (MAE), confirming spatial extent used to aggregate NDVI data strongly influences model accuracy. No significant differences observed across NDVI metrics for RMSE ($p = 0.1355$) or MAE ($p = 0.2096$), suggesting errors are less sensitive to metric choice. However, for R^2, the pattern reverses: no significant variation across scales ($p = 0.5464$), but NDVI metrics significantly affect explanatory power ($p = 0.0110$). This implies while different metrics yield similar error magnitudes, they differ in reproducing observed groundwater variability, with metrics like maximum NDVI providing stronger alignment with observed dynamics.

For well P2, extraction scale significantly affects MAE ($p = 0.0356$) but not RMSE ($p = 0.0891$) or R^2 ($p = 0.7821$). NDVI metrics show no significant effect on any indicator

(RMSE: $p = 0.4523$; MAE: $p = 0.6201$; R^2: $p = 0.2145$), suggesting for P2, scale matters more than metric choice, particularly at intermediate 1000 m buffer.

Table 4. Kruskal–Wallis test results for RMSE, MAE, and R^2 across NDVI extraction scales and statistical metrics. Bold values indicate statistical significance at $\alpha = 0.05$.

Well	Metric	By Scale *p*-Value	By Metric *p*-Value
P1	RMSE	0.020	0.135
P1	MAE	0.009	0.209
P1	R^2	0.546	0.011
P2	RMSE	0.089	0.452
P2	MAE	0.036	0.620
P2	R^2	0.782	0.215
P3	RMSE	0.017	0.188
P3	MAE	0.009	0.301
P3	R^2	0.489	0.023
P4	RMSE	0.001	0.562
P4	MAE	0.001	0.679
P4	R^2	0.005	0.346

For well P3, extraction scale significantly affects both RMSE ($p = 0.0167$) and MAE ($p = 0.0089$), with no significant R^2 effect ($p = 0.4892$). NDVI metrics significantly affect R^2 ($p = 0.0234$) but not RMSE ($p = 0.1876$) or MAE ($p = 0.3012$). This pattern mirrors P1, where scale controls error magnitude while metric choice influences explanatory power.

For well P4, extraction scale shows highly significant effect on all three indicators (RMSE: $p = 0.0012$; MAE: $p = 0.0008$; R^2: $p = 0.0045$), indicating scale is dominant factor. NDVI metrics show no significant effect (RMSE: $p = 0.5621$; MAE: $p = 0.6789$; R^2: $p = 0.3456$).

Overall, extraction scale consistently emerges as significant factor affecting prediction errors across wells, particularly P1, P3, P4. NDVI metric effects are more variable and well-specific, with significant R^2 effects for P1, P3 but not P2, P4. These results confirm spatial scale optimization is critical for all wells, while metric selection requires site-specific consideration.

3.4. Spatial Validation Results

Spatial distribution of irrigated areas (NDVI > 0.45) was analyzed across six buffer scales for four representative drought years. These dates, previously identified as driest summer periods over 2000–2020, provide insight into irrigation activity under water stress. Table 5 presents results for well P1, with corresponding data for P2, P3, P4 in Table S9 (Supplementary Material).

Table 5. Evolution of irrigated area by extraction scale and drought period for Well P1. Irrigated area expressed in km^2.

Scale (m)	28 July 2001	12 July 2005	12 July 2010	28 July 2017
500	0.163	0.243	0.762	0.760
1000	1.1	1.9	3.0	3.0
2500	8.5	13.3	16.6	15.9
10,000	85.1	149.8	189.4	193.1
15,000	150.1	265.8	362.6	382.0
20,000	201.3	369.6	494.5	522.9

For well P1, general increase in irrigated surface area occurs over time. At smallest scales (500, 1000 m), irrigated area grows between 2001 and 2010, then stabilizes in 2017.

At 2500 m scale, irrigated area increased substantially between 2001 and 2010, reaching a maximum 16.64 km^2, before slightly decreasing to 15.87 km^2 in 2017. At larger scales (10,000, 15,000, 20,000 m), irrigated surfaces more than doubled between 2001 and 2017, reflecting substantial regional irrigation expansion. For example, at 15,000 m scale, NDVI > 0.45 area increased from 150.1 km^2 (2001) to 382.0 km^2 (2017).

Similar trends of increasing irrigated area over time occur for wells P2, P3, P4, though absolute values differ based on well location within irrigated perimeter (Table S9). Wells located in more intensively irrigated zones show higher baseline irrigated areas even at smaller buffer scales.

Figure 7 presents the spatial validation analysis for wells P1, P2, P3, and P4, comparing irrigated area, NDVI extraction scale, NDVI values, and model performance across the four NDVI metrics. Model performance is evaluated using RMSE (Root Mean Square Error), MAE (Mean Absolute Error), and R^2 (coefficient of determination). Overall, larger extraction scales generally capture larger irrigated areas and are associated with improved model performance, although the optimal scale varies among wells. For P1, the maximum NDVI metric provides the best performance at the 15,000 m scale, where the average irrigated area reaches 290.14 km^2, with RMSE = 0.09 m, MAE = 0.07 m, and R^2 = 0.99. Similar improvements with increasing extraction scale are observed for P3 and P4, which also show their best performance at larger buffers. In contrast, P2 reaches its optimal performance at the 1000 m scale, while still showing strong performance at larger scales, indicating that the most informative NDVI extraction scale may vary depending on the local context of each well.

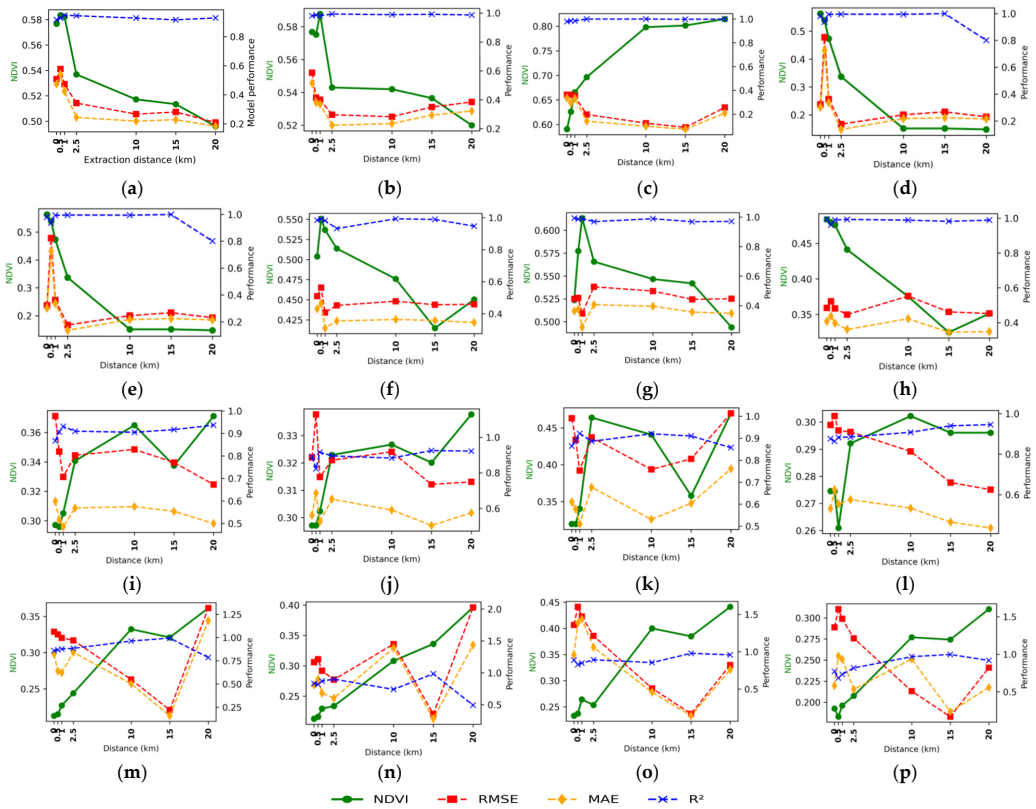

Figure 7. Spatial validation of NDVI-derived irrigated areas and model performance for wells P1, P2, P3, and P4. Results are presented for well P1 using (**a**) mean NDVI, (**b**) median NDVI, (**c**) maximum NDVI, and (**d**) minimum NDVI; well P2 using (**e**) mean NDVI, (**f**) median NDVI, (**g**) maximum NDVI, and (**h**) minimum NDVI; well P3 using (**i**) mean NDVI, (**j**) median NDVI, (**k**) maximum NDVI, and (**l**) minimum NDVI; and well P4 using (**m**) mean NDVI, (**n**) median NDVI, (**o**) maximum NDVI, and (**p**) minimum NDVI.

Across the four wells, the spatial validation supports the interpretation that broader buffers can better capture the regional vegetation signal associated with irrigated areas. However, this relationship should not be interpreted as direct evidence of irrigation volumes or groundwater abstraction, since pumping rates and measured irrigation water use were not available. The results therefore indicate that larger NDVI extraction scales generally provide useful spatial information for groundwater level prediction, while also showing that well-specific differences can influence the optimal extraction scale.

4. Discussion

4.1. NDVI Spatial Scale Sensitivity in Capturing Irrigation-Driven Groundwater Variations

Results show that NDVI extraction spatial scale has a strong influence on groundwater level prediction accuracy across the four monitoring wells. Larger extraction scales, particularly those exceeding 2500 m, generally show stronger correlations with groundwater level fluctuations and improved predictive performance. For wells P1, P3, and P4, the most accurate predictions are achieved at the 15,000 m scale, while well P2 shows optimal performance at 1000 m, followed by strong performance at 15,000 m (Table 4). For P1, this scale yields the lowest RMSE (0.09 m) and MAE (0.07 m), with a near-perfect R^2 of 0.99. For P4, similarly high performance is achieved at 15,000 m, with RMSE = 0.168 m, MAE = 0.142 m, and R^2 = 0.979. This improvement coincides with a marked increase in irrigated surface area, identified using the NDVI > 0.45 threshold, captured within larger buffers. Spatial validation shows that these irrigated areas more than doubled between 2001 and 2017, indicating substantial irrigation expansion during drought years [57]. These patterns suggest that broader extraction zones may better capture cumulative vegetation signals associated with irrigated areas, especially under water-stressed conditions where persistent NDVI values above 0.45 are more likely to reflect irrigation-dependent vegetation cover [8,56,58,59]. However, this interpretation should be considered as indirect evidence, since direct irrigation volumes, pumping data, and field-based abstraction measurements were not available. In addition, part of the improved performance at larger scales may also result from spatial aggregation and statistical smoothing of the NDVI signal, which can reduce local variability and noise. From a management perspective, these findings suggest that groundwater level variations observed at monitoring wells may be more strongly associated with broader NDVI patterns related to irrigated areas than with vegetation conditions immediately surrounding each well. This interpretation is consistent with irrigation practices in semi-arid regions, where groundwater can be pumped and transported away from its source through plastic pipes, traditional open-air canals, seguias, or concrete channels (Figure 8a,b), to irrigate fields located hundreds or thousands of meters away [60–63]. In some cases, water is stored in small reservoirs before redistribution according to demand (Figure 8c). Such decentralized irrigation practices are common in the Tadla plain, where gravity-based irrigation remains dominant [41–44]. The Tadla Regional Agricultural Development Office manages a gravity-fed network extending over 2630 km, enabling water redistribution to multiple plots, often far from the original well location [64].

These patterns may also be consistent with spatial variability in groundwater abstraction intensity across the perimeter. As shown in Figure 8d, some farms operate multiple high-capacity pumps almost continuously, leading to localized overexploitation [59,65], whereas others depend on a single low-powered motor running intermittently. Such uneven pumping intensity may contribute to spatial heterogeneity in groundwater responses, although the available data do not allow this mechanism to be directly quantified [66,67]. The better performance of wells P1, P3, and P4 at the 15,000 m extraction scale may therefore reflect the ability of larger buffers to capture broader vegetation signals associated with dispersed irrigation activities. However, part of this improvement may also result from spatial

aggregation and statistical smoothing of NDVI values, which can reduce local variability and noise. The case of well P2, which performs optimally at the 1000 m scale, suggests that the local NDVI signal may be more informative for this well than broader-scale vegetation patterns. However, the available data do not allow this behavior to be attributed to a specific mechanism. Alternative explanations, including local hydrogeological conditions, depth to the water table, recharge characteristics, or land-use patterns around the well, may also contribute to this observed scale sensitivity. The increasing prevalence of individually managed wells, operating independently of collective irrigation systems [60,68,69], may further contribute to spatially variable irrigation and groundwater-use patterns.



Figure 8. Field photographs taken in June 2025 showing: (**a**) Irrigation water distribution canals (modern concrete channels). (**b**) Traditional seguia channel (open-air earthen canal). (**c**) Open-air reservoirs for groundwater storage before redistribution. (**d**) Modern groundwater abstraction system powered by solar panels.

The effectiveness of larger NDVI extraction scales in our study is consistent with findings from other domains, such as environmental health and urban planning, where broader spatial windows have yielded stronger associations with ecological and anthropogenic processes by reducing spatial misclassification and better representing landscape variability [17,18,20,70]. While most of those studies used relatively small buffers, 100–500 m, their conclusions parallel our results, where accuracy generally improves as extraction scale increases from 500 m to 15,000 m. This is consistent with the established scale-dependence of NDVI relationships with environmental variables such as vegetation cover, topography, and climate [71–73]. In heterogeneous agricultural landscapes like Tadla, buffer size influences the NDVI signal extracted around wells and, consequently, may affect groundwater model predictive accuracy. Larger buffers in our analysis, extending several kilometers,

therefore appear more suitable for capturing cumulative vegetation signals associated with regional irrigation activity, while also potentially reducing noise through spatial averaging [12,74–76].

Finally, the link between scale-dependent NDVI–groundwater relationships and well-specific groundwater responses should be interpreted with caution. Wells P1, P3, and P4 all show optimal performance at 15,000 m, suggesting that their groundwater level variations may be better represented by broader NDVI signals associated with regional irrigation activity rather than by strictly local vegetation conditions. In contrast, well P2 performs optimally at the 1000 m scale, while still showing strong performance at 15,000 m, indicating that the local NDVI signal may be more informative for this well. These well-specific differences highlight the need to consider both extraction scale and local context when selecting NDVI inputs for groundwater level forecasting.

4.2. Relevance of Maximum and Median NDVI Metrics for Monitoring Groundwater Dynamics in Irrigated Semi-Arid Areas

Performance of different NDVI metrics varies across the four monitoring wells, revealing both consistent patterns and site-specific preferences. The strong performance of the maximum NDVI metric for wells P1, P2, and P4 is notable. At their optimal scales, maximum NDVI achieved high predictive accuracy for P1, with RMSE = 0.09 m, MAE = 0.07 m, and R^2 = 0.99, and for P4, with RMSE = 0.168 m, MAE = 0.142 m, and R^2 = 0.979, while also performing strongly for P2 at 1000 m, with RMSE = 0.347 m, MAE = 0.254 m, and R^2 = 0.99. This pattern is consistent with the agro-climatic context of the study area, characterized by recurrent drought and intensive irrigation, where high NDVI peaks are more likely to represent irrigated crops than rainfed vegetation [8,77]. This distinction holds not only during drought years but throughout the growing season, as irrigated fields generally maintain higher NDVI values compared to non-irrigated ones [78]. In the Tadla region, previous research has shown the usefulness of maximum NDVI for distinguishing irrigated plots during peak vegetation periods [31,79]. By capturing the highest levels of photosynthetic activity, biomass, and vegetation cover, maximum NDVI may therefore provide a useful proxy for vegetation patterns associated with sustained irrigation activity, especially during drought periods [11,12,77,80].

Interestingly, P3 shows a contrasting pattern, where the minimum NDVI metric outperforms the other metrics at larger scales, especially at 15,000 m, with RMSE = 0.625 m, MAE = 0.465 m, and R^2 = 0.940. This suggests that, for P3, vegetation stress indicators or the extent of bare or sparsely vegetated areas within the buffer may provide more relevant information for groundwater level prediction than peak greenness. This could be related to differences in crop types, irrigation practices, or local environmental conditions around this location, although aquifer response characteristics cannot be confirmed without detailed well-specific hydrogeological data. Minimum NDVI may be particularly sensitive to areas where irrigation has ceased or where vegetation stress is more pronounced, thus serving as a potential indicator of water scarcity rather than water use intensity.

The median NDVI metric showed consistently solid performance across spatial scales for most wells, ranking just behind maximum NDVI in most cases. For example, for P1, at scales between 2500 and 15,000 m, median NDVI predictions clustered closely around observed data points in Taylor diagrams, reflecting stable predictive accuracy even when maximum NDVI was slightly superior. This stability arises from its ability to reduce the influence of extreme values caused by noise, cloud contamination, or irregular surface conditions, which are common challenges in satellite-based time series [26,81,82]. In highly variable environments such as semi-arid irrigated zones, the median provides a more robust measure of central tendency and reduces the distorting effect of abnormally wet or dry years [83]. Across the four wells, model performance with median NDVI generally

improved with scale, particularly beyond 2500 m, supporting its value as a noise-resistant metric for capturing vegetation dynamics potentially associated with groundwater use.

By contrast, mean NDVI generally ranked among the lowest metrics in predictive accuracy across most wells and scales, with RMSE values up to 0.58 m and MAE up to 0.54 m for P1. This may be related to its averaging process, which smooths local extremes and reduces the influence of spatial variability [83–85]. As a result, mean NDVI may obscure localized irrigation-related vegetation signals, reducing its ability to represent spatial heterogeneity in semi-arid agricultural landscapes [86]. The minimum NDVI metric produced mixed results across wells, performing well for P3 at intermediate to large scales, notably 15,000 m, with RMSE = 0.625 m, but showing higher variability for P1, with RMSE up to 0.82 m, and for P4, particularly at very small or very large buffers. This suggests that minimum NDVI may be useful in specific contexts where vegetation stress or reduced irrigation signals are informative, but its reliability varies with local conditions and spatial extent.

Overall, maximum NDVI appears to be the most robust metric across the monitored wells, as it captures peak vegetation activity associated with irrigation during critical growing periods. Median NDVI offers a valuable alternative where data quality concerns exist or where consistent performance across scales is prioritized over absolute accuracy. Mean NDVI, despite its widespread use, appears less suitable for groundwater level prediction in heterogeneous irrigated landscapes. Minimum NDVI shows potential in specific contexts, such as P3, where stress-related vegetation signals may be relevant, but it requires careful site-specific evaluation.

4.3. Implications for Groundwater Monitoring and Management

This study provides several practical implications for groundwater monitoring in irrigated semi-arid regions. First, the better performance of large-scale NDVI extraction, particularly the 15,000 m buffer for most wells, suggests that groundwater monitoring approaches using remote sensing data should consider broader vegetation signals rather than relying only on vegetation conditions immediately surrounding each well. This indicates that regional-scale NDVI patterns may provide more informative inputs for predicting groundwater level variations.

Second, the case of well P2, which performs optimally with small-scale NDVI at 1000 m, suggests that some wells may be better represented by more local vegetation signals. Therefore, optimal NDVI extraction strategies should be adapted to well-specific responses and surrounding land-use patterns rather than applying a uniform extraction scale across an entire monitoring network.

Third, the strong performance of maximum NDVI across three of the four wells, P1, P2, and P4, provides practical guidance for operational groundwater monitoring systems. Maximum NDVI composites are readily available from standard satellite products and require limited preprocessing, making them a useful option for water management agencies with limited data availability. However, the better performance of minimum NDVI for well P3 suggests that, in some local contexts, particularly where vegetation stress or reduced irrigation signals are relevant, alternative metrics may provide complementary information.

Fourth, the doubling of irrigated area during the 2001–2017 drought period, as revealed by spatial validation, suggests increasing pressure on groundwater resources. This expansion occurred despite declining water tables (Table 1), indicating a potentially unsustainable adaptation strategy in the long term. The relationship between captured irrigated area and model performance suggests that remote sensing-based monitoring can help track this expansion and provide indirect indicators of increasing pressure on groundwater resources.

4.4. Methodological Considerations and Transferability

The LSTM approach demonstrated in this study achieved high predictive accuracy, with R^2 values ranging from 0.94 to 0.997, while relying on a relatively simple input structure based on NDVI time series and historical groundwater levels. This parsimonious framework may be transferable to other irrigated regions where groundwater monitoring data are available but where detailed information on irrigation practices, pumping rates, or crop types remains limited. However, the high model performance should be interpreted with caution, as it may partly reflect the strong temporal structure of groundwater level series, the use of spatially aggregated NDVI inputs, and the specific characteristics of the Tadla irrigated plain. The systematic evaluation of 96 models across different extraction scales and metrics provides a useful methodological template for selecting appropriate NDVI configurations in new study areas.

Several factors may influence transferability. The Tadla Plain has a well-developed irrigation system and relatively extensive irrigated areas, which may favor strong associations between NDVI signals and groundwater level variations. In regions with more complex hydrogeological settings, such as fractured aquifers, highly heterogeneous multilayer systems, or areas where rainfed and irrigated agriculture are strongly intermixed, optimal scales and metrics may differ. In addition, the 250 m MODIS resolution used here represents a trade-off between spatial detail and temporal frequency. In regions with smaller field sizes or more fragmented agricultural landscapes, higher-resolution sensors such as Sentinel-2 at 10 m may be more appropriate, although this would require redefining buffer sizes and testing scale effects accordingly.

The study's focus on drought years, 2001, 2005, 2010, and 2017, for spatial validation was intended to emphasize periods when irrigation-dependent vegetation is more distinguishable from rainfed or natural vegetation. In regions with more balanced precipitation regimes or different irrigation calendars, alternative validation approaches using multiple seasonal snapshots may be more appropriate. Similarly, the NDVI > 0.45 threshold used to identify irrigated areas, although supported by previous studies in semi-arid environments, should be calibrated and validated under local conditions before being applied elsewhere.

4.5. Study Limitations and Future Directions

Several limitations warrant consideration. First, the 10-year study period, 2009–2018, while encompassing important drought conditions, may not capture the full range of climate variability or long-term trends. Extending the analysis to longer time periods would enable assessment of model performance under contrasting wet and dry cycles.

Second, the four-well network, while providing valuable spatial coverage, represents a limited sample size for generalizing across the entire 320,000 ha aquifer. The selected wells were chosen because they provide the longest and most complete observation records available within the Tadla irrigated perimeter and because they are located in irrigated areas. However, detailed borehole metadata were not available, which is a common limitation of institutional piezometric datasets. In this study, the available records mainly consisted of depth-to-water measurements, later converted into groundwater level time series. This limits the interpretation of local hydrogeological controls on model performance. Expanding the analysis to additional wells, particularly in transitional zones between intensive and moderate irrigation, would strengthen conclusions about optimal scale selection.

Third, this study focused exclusively on NDVI as the input variable. While this design choice enabled systematic evaluation of scale and metric effects, incorporating additional remote sensing variables, such as land surface temperature, evapotranspiration, or soil moisture, could potentially improve predictions and provide complementary information about irrigation water use. In addition, the improved performance observed at larger

NDVI extraction scales should not be interpreted solely as evidence of hydrogeological processes. Larger buffers may also reduce local variability and noise through spatial averaging, producing smoother and more stable NDVI time series. Therefore, part of the observed scale effect may reflect statistical smoothing and spatial aggregation, in addition to broader irrigation-related groundwater signals. Fourth, the absence of actual pumping rate or irrigation volume data limits the ability to directly validate relationships between NDVI signals and water extraction. Future research integrating metered pumping data with remote sensing observations would enable a more mechanistic understanding of scale-dependent relationships.

Fifth, the LSTM models, while achieving excellent predictive performance, function as black boxes with limited interpretability compared to process-based groundwater models. Although several models achieved very high R^2 values, these results should be interpreted with caution. The relatively short validation period and the limited number of wells may reduce the ability to fully assess model generalization under contrasting hydroclimatic conditions. While dropout regularization and hyperparameter tuning were used to reduce overfitting, future studies should test model robustness using longer independent validation periods, larger monitoring networks, and external validation datasets. Hybrid approaches combining physically based modeling with data-driven components could potentially provide both accuracy and mechanistic insight.

Finally, the study's focus on monthly time steps may obscure important sub-monthly dynamics during critical irrigation periods. Higher temporal frequency analysis using daily or weekly data could reveal additional insights about lag times between irrigation events and groundwater response.

Future research should address these limitations by: (1) extending temporal coverage to more than 20 years to capture multiple climate cycles; (2) expanding spatial coverage to larger well networks and diverse hydrogeological settings; (3) implementing multi-variable remote sensing inputs beyond NDVI alone; (4) separating the effects of hydrogeological processes from statistical smoothing caused by spatial aggregation; (5) validating against ground-truth irrigation and pumping data where available; (6) developing hybrid models combining LSTM with process-based components; (7) exploring higher temporal resolution analysis to capture sub-monthly dynamics; and (8) assessing climate change impacts on optimal NDVI scales as irrigation patterns shift. Additionally, applying this methodology to other irrigated regions globally would test its broader applicability and potentially reveal new insights about irrigation–groundwater relationships across diverse contexts.

5. Conclusions

This study systematically evaluated how NDVI extraction spatial scale and statistical metric choice influence groundwater level prediction accuracy using LSTM neural networks in Morocco's semi-arid Tadla irrigation plain. Analysis of 96 models across four monitoring wells revealed a consistent and coherent picture of the factors governing model performance.

This study systematically evaluated how NDVI extraction spatial scale and statistical metric choice influence groundwater level prediction accuracy using LSTM neural networks in Morocco's semi-arid Tadla irrigation plain. Analysis of 96 models across four monitoring wells revealed a consistent pattern showing that both extraction scale and metric selection strongly affect model performance.

Spatial scale emerged as a key factor influencing prediction accuracy. Larger NDVI extraction buffers ($\geq$2500 m) generally outperformed smaller scales ($\leq$1000 m), with optimal performance achieved at 15,000 m for three of the four wells (P1, P3, and P4). Kruskal–Wallis tests confirmed that extraction scale significantly affects prediction errors ($p < 0.05$) for

most wells. This pattern coincides with the extent of irrigated area captured within larger buffers, which more than doubled during the 2001–2017 drought period. However, this result should not be interpreted as direct evidence of a specific hydrogeological mechanism. Rather, it suggests that groundwater level prediction in the Tadla plain is more strongly associated with broader NDVI signals linked to irrigated vegetation than with strictly local vegetation conditions around individual wells. Part of the improved performance at larger scales may also result from spatial aggregation and statistical smoothing of NDVI time series.

The choice of statistical metric was also important, although the optimal configuration varied among wells. Maximum NDVI yielded the best results for wells P1, P2, and P4, achieving high predictive accuracy (RMSE: 0.09–0.347 m; R^2: 0.979–0.997), likely because it captures peak vegetation activity associated with irrigation during critical growing periods. Median NDVI provided a stable and consistent alternative across spatial scales. However, the contrasting behavior of well P2, whose optimal performance occurred at 1000 m rather than 15,000 m, and well P3, which responded most strongly to minimum NDVI, indicates that optimal scale–metric configurations may vary according to local context. Detailed borehole-level information, pumping data, and hydraulic properties would be required to confirm the mechanisms behind these differences.

Taken together, these results carry important methodological and operational implications. The need to jointly optimize both spatial scale and statistical metric challenges the use of arbitrary buffer sizes or default averaging methods in remote sensing-based hydrological studies. From a practical standpoint, the LSTM framework achieved high predictive accuracy ($R^2 > 0.94$) using only NDVI time series and historical groundwater records. This suggests that NDVI-based deep learning models can provide a useful and resource-efficient support tool for groundwater monitoring in data-scarce irrigated regions, while recognizing that further validation is needed before broader operational transfer.

Based on these findings, several recommendations can be drawn: (i) NDVI extraction scale should not be selected arbitrarily, as larger buffers generally provide more reliable groundwater level predictions in irrigated semi-arid settings; (ii) maximum NDVI can be prioritized when the objective is to capture peak vegetation activity associated with irrigation, while alternative metrics should also be tested; (iii) multi-scale NDVI testing should be systematically included before applying deep learning models to groundwater forecasting; and (iv) water management agencies may use NDVI-based LSTM models as a cost-effective complementary monitoring tool in data-scarce irrigated regions.

Future research should extend this approach to longer observational periods and broader monitoring networks, while integrating complementary remote sensing variables, pumping data, irrigation volumes, and local hydrogeological information where available. Such developments would help distinguish the respective roles of hydrogeological processes, irrigation practices, and statistical smoothing in scale-dependent NDVI–groundwater relationships.

Supplementary Materials: The following supporting information can be downloaded at: https://www.mdpi.com/article/10.3390/hydrology13070192/s1, Figure S1. Temporal NDVI variations for well P2 across the different extraction scales. Monthly NDVI time series for the period 2009–2018 are shown for the seven extraction scales: 0 m, 500 m, 1000 m, 2500 m, 10,000 m, 15,000 m, and 20,000 m. Panels show: (a) mean NDVI; (b) median NDVI; (c) maximum NDVI; (d) minimum NDVI. Figure S2. Temporal NDVI variations for well P3 across the different extraction scales. Monthly NDVI time series for the period 2009–2018 are shown for the seven extraction scales: 0 m, 500 m, 1000 m, 2500 m, 10,000 m, 15,000 m, and 20,000 m. Panels show: (a) mean NDVI; (b) median NDVI; (c) maximum NDVI; (d) minimum NDVI. Figure S3. Temporal NDVI variations for well P4 across the different extraction scales. Monthly NDVI time series for the period 2009–2018 are shown for

the seven extraction scales: 0 m, 500 m, 1000 m, 2500 m, 10,000 m, 15,000 m, and 20,000 m. Panels show: (a) mean NDVI; (b) median NDVI; (c) maximum NDVI; (d) minimum NDVI. Figure S4: Taylor diagrams showing model performance across NDVI extraction scales for wells P2; Panels show the results for well P1 using (a) mean NDVI, (b) median NDVI, (c) maximum NDVI, and (d) minimum NDVI; Figure S5: Taylor diagrams showing model performance across NDVI extraction scales for wells P3; Panels show the results for well P1 using (a) mean NDVI, (b) median NDVI, (c) maximum NDVI, and (d) minimum NDVI; Figure S6: Taylor diagrams showing model performance across NDVI extraction scales for wells P4; Panels show the results for well P1 using (a) mean NDVI, (b) median NDVI, (c) maximum NDVI, and (d) minimum NDVI; Table S1: Prediction performance metrics for well P1; Table S2: Mean performance metrics by extraction scale and NDVI metric for well P1; Table S3: Prediction performance metrics for well P2; Table S4: Mean performance metrics by extraction scale and NDVI metric for well P2; Table S5: Prediction performance metrics for well P3; Table S6: Mean performance metrics by extraction scale and NDVI metric for well P3; Table S7: Prediction performance metrics for well P4; Table S8: Mean performance metrics by extraction scale and NDVI metric for well P4; Table S9: Evolution of irrigated area by extraction scale and drought period for wells P2, P3, and P4.

Author Contributions: Conceptualization, H.H., T.B., I.K. and M.L.; methodology, H.H., N.K. (Nourelhouda Karmouda), T.B. and Y.H.-A.; software, H.H. and N.K. (Nourelhouda Karmouda); validation, T.B., I.M., I.K. and M.L.; formal analysis, H.H., N.K. (Nourelhouda Karmouda) and Y.H.-A.; investigation, H.H., H.B. and H.M.; resources, H.B., H.M., M.T., N.K. (Nadia Kassou) and I.K.; data curation, H.H., T.B., I.K. and M.L.; writing—original draft preparation, H.H. and T.B.; writing—review and editing, T.B., I.M., M.T., N.K. (Nadia Kassou), I.K. and M.L.; visualization, H.H. and Y.H.-A.; supervision, T.B., I.K. and M.L.; project administration, T.B. and M.L.; funding acquisition, M.L. All authors have read and agreed to the published version of the manuscript.

Funding: The APC was funded by the JEAI PESAS, a joint research collaboration between the University of Mohammed V, Avignon University and the IRD.

Data Availability Statement: The data are available from the corresponding author upon reasonable request.

Acknowledgments: This work was supported by the JEAI PESAS, a joint research collaboration between the University of Mohammed V, Avignon University and the IRD. The authors acknowledge the Oum Er-Rbia Hydraulic Basin Agency for providing groundwater monitoring data and the NASA Land Processes Distributed Active Archive Center (LP DAAC) for MODIS NDVI data.

Conflicts of Interest: The authors declare no conflicts of interest.

Abbreviations

The following abbreviations are used in this manuscript:

NDVI	Normalized Difference Vegetation Index
LSTM	Long Short-Term Memory
RNN	Recurrent Neural Network
CEC	Constant Error Carousel
MODIS	Moderate Resolution Imaging Spectroradiometer
MOD13Q1	MODIS/Terra Vegetation Indices 16-Day L3 Global 250 m product
GRACE	Gravity Recovery and Climate Experiment
RMSE	Root Mean Squared Error
MAE	Mean Absolute Error
R^2	Coefficient of determination
MSE	Mean Squared Error
SD	Standard Deviation
LST	Land Surface Temperature
ET	Evapotranspiration

References

1. Zamani, M.G.; Moridi, A.; Yazdi, J. Groundwater management in arid and semi-arid regions. *Arab. J. Geosci.* **2022**, *15*, 362. [CrossRef]
2. Yan, H.; Xie, Z.; Jia, B.; Li, R.; Wang, L.; Tian, Y.; You, Y. Impact of groundwater overextraction and agricultural irrigation on hydrological processes in an inland arid basin. *J. Hydrol.* **2025**, *645*, 132770. [CrossRef]
3. Abidi, J.H.; Elzain, H.E.; Sabarathinam, C.; El Fehri, R.M.; Farhat, B.; Mammou, A.B.; Senapathi, V. Integrated approach to understand the multiple natural and anthropogenic stresses on intensively irrigated coastal aquifer in the Mediterranean region. *Environ. Res.* **2024**, *252*, 118757. [CrossRef] [PubMed]
4. Bulcock, H.H.; Jewitt, G.P.W. Spatial mapping of leaf area index using hyperspectral remote sensing for hydrological applications with a particular focus on canopy interception. *Hydrol. Earth Syst. Sci.* **2010**, *14*, 383–392. [CrossRef]
5. Otto, M.; Scherer, D.; Richters, J. Hydrological differentiation and spatial distribution of high altitude wetlands in a semi-arid Andean region derived from satellite data. *Hydrol. Earth Syst. Sci.* **2011**, *15*, 1713–1727. [CrossRef]
6. Parizi, E.; Hosseini, S.M.; Ataie-Ashtiani, B.; Simmons, C.T. Normalized difference vegetation index as the dominant predicting factor of groundwater recharge in phreatic aquifers: Case studies across Iran. *Sci. Rep.* **2020**, *10*, 17473. [CrossRef] [PubMed]
7. Mohajane, M.; Essahlaoui, A.; Oudija, F.; Hafyani, M.E.; Hmaidi, A.E.; Ouali, A.E.; Teodoro, A.C. Land use/land cover using Landsat data series in Azrou Forest, in the Central Middle Atlas of Morocco. *Environments* **2018**, *5*, 131. [CrossRef]
8. Pervez, M.S.; Budde, M.; Rowland, J. Mapping irrigated areas in Afghanistan over the past decade using MODIS NDVI. *Remote Sens. Environ.* **2014**, *149*, 155–165. [CrossRef]
9. Grados, D.; Reynarfaje, X.; Schrevens, E. A methodological approach to assess canopy NDVI-based tomato dynamics under irrigation treatments. *Agric. Water Manag.* **2020**, *240*, 106208. [CrossRef]
10. Li, W.; Finsa, M.M.; Laskey, K.B.; Houser, P.; Douglas-Bate, R. Groundwater level prediction with machine learning to support sustainable irrigation in water scarcity regions. *Water* **2023**, *15*, 3473. [CrossRef]
11. Bouramtane, T.; Tiouiouine, A.; Kacimi, I.; Valles, V.; Talih, A.; Kassou, N.; Ouardi, J.; Saidi, M.E.M.; Morarech, M.; Yameogo, S.; et al. Drainage network patterns determinism: A comparison in arid, semi-arid and semi-humid area of Morocco using multifactorial approach. *Hydrology* **2020**, *7*, 87. [CrossRef]
12. Bouramtane, T.; Mohsine, I.; Karmouda, N.; Leblanc, M.; Estève, Y.; Kacimi, I.; Chafki, O. Dimensionality reduction for groundwater forecasting under drought and intensive irrigation with neural networks. *J. Hydrol. Reg. Stud.* **2025**, *60*, 102477. [CrossRef]
13. Elmotawakkil, A.; Sadiki, A.; Enneya, N. Predicting groundwater level based on remote sensing and machine learning: A case study in the Rabat-Kénitra region. *J. Hydroinform.* **2024**, *26*, 2639–2667. [CrossRef]
14. Marchetti, Z.Y.; Minotti, P.G.; Ramonell, C.G.; Schivo, F.; Kandus, P. NDVI patterns as indicator of morphodynamic activity in the middle Paraná River floodplain. *Geomorphology* **2016**, *253*, 146–158. [CrossRef]
15. Hassan, M.A.; Yang, M.; Rasheed, A.; Yang, G.; Reynolds, M.; Xia, X. A rapid monitoring of NDVI across the wheat growth cycle for grain yield prediction using a multi-spectral UAV platform. *Plant Sci.* **2019**, *282*, 95–103. [CrossRef] [PubMed]
16. Hamou-Ali, K.; Bouramtane, T.; Kacimi, I.; Leblanc, M.; Abraham, S.; Raclot, D.; Taky, A. Downscaling GRACE total water storage using machine learning and remote sensing in Morocco. *Hydrol. Sci. J.* **2025**, *in press*. [CrossRef]
17. Su, J.G.; Dadvand, P.; Nieuwenhuijsen, M.J.; Bartoll, X.; Jerrett, M. Associations of green space metrics with health and behavior outcomes at different buffer sizes and remote sensing sensor resolutions. *Environ. Int.* **2019**, *126*, 162–170. [CrossRef] [PubMed]
18. Gascon, M.; Cirach, M.; Martínez, D.; Dadvand, P.; Valentín, A.; Plasència, A.; Nieuwenhuijsen, M.J. Normalized difference vegetation index as a marker of surrounding greenness in epidemiological studies: The case of Barcelona city. *Urban For. Urban Green* **2016**, *19*, 88–94. [CrossRef]
19. De La Iglesia Martinez, A.; Labib, S.M. Demystifying normalized difference vegetation index for greenness exposure assessments and policy interventions in urban greening. *Environ. Res.* **2023**, *220*, 115155. [CrossRef]
20. Rugel, E.J.; Henderson, S.B.; Carpiano, R.M.; Brauer, M. Beyond the normalized difference vegetation index: Developing a natural space index for population-level health research. *Environ. Res.* **2017**, *159*, 474–483. [CrossRef] [PubMed]
21. Chen, Y.; Lu, D.; Luo, L.; Pokhrel, Y.; Deb, K.; Huang, J.; Ran, Y. Detecting irrigation extent, frequency, and timing in a heterogeneous arid agricultural region using MODIS time series, Landsat imagery, and ancillary data. *Remote Sens. Environ.* **2018**, *204*, 197–211. [CrossRef]
22. Foster, T.; Gonçalves, I.Z.; Campos, I.; Neale, C.M.U.; Brozović, N. Assessing landscape scale heterogeneity in irrigation water use with remote sensing and in situ monitoring. *Environ. Res. Lett.* **2019**, *14*, 024004. [CrossRef]
23. Tan, M.; Ran, Y.; Feng, M.; Dong, G.; Du, D.; Zhu, G.; Li, X. Long-term monitoring of the annual irrigated cropland extent in fragmented and heterogeneous arid landscapes using machine learning and Landsat imagery. *Water Resour. Res.* **2024**, *60*, e2023WR036945. [CrossRef]
24. Hill, M.J.; Donald, G.E. Estimating spatio-temporal patterns of agricultural productivity in fragmented landscapes using AVHRR NDVI time series. *Remote Sens. Environ.* **2003**, *84*, 367–384. [CrossRef]

25. Alcaraz-Segura, D.; Cabello, J.; Paruelo, J. Baseline characterization of major Iberian vegetation types based on the NDVI dynamics. *Plant Ecol.* **2009**, *202*, 13–29.
26. Hird, J.N.; McDermid, G.J. Noise reduction of NDVI time series: An empirical comparison of selected techniques. *Remote Sens. Environ.* **2009**, *113*, 248–258. [CrossRef]
27. Martínez, B.; Gilabert, M.A. Vegetation dynamics from NDVI time series analysis using the wavelet transform. *Remote Sens. Environ.* **2009**, *113*, 1823–1842. [CrossRef]
28. Liu, R. Compositing the minimum NDVI for MODIS data. *IEEE Trans. Geosci. Remote Sens.* **2016**, *55*, 1396–1406.
29. Wilton, M. Crop Yield Estimation Using NDVI: A Comparison of Various NDVI Metrics. Master Thesis, University of British Columbia, Vancouver, BC, Canada, 2021.
30. Lionboui, H.; Benabdelouahab, T.; Elame, F.; Boudhar, A.; Salhi, A.; Hadria, R. The contribution of the costs of agricultural inputs to wheat grain yield: Morocco as a case study. In *Recent Advances in Environmental Science from the Euro-Mediterranean and Surrounding Regions*, 2nd ed.; Ksibi, M., Sousa, A., Hentati, O., Chenchouni, H., Lopes Velho , J., Negm, A., Rodrigo-Comino, J., Eds.; Springer International Publishing: Cham, Switzerland, 2021; pp. 1169–1173.
31. Lebrini, Y.; Boudhar, A.; Htitiou, A.; Hadria, R.; Lionboui, H.; Bounoua, L.; Benabdelouahab, T. Remote monitoring of agricultural systems using NDVI time series and machine learning methods: A tool for an adaptive agricultural policy. *Arab. J. Geosci.* **2020**, *13*, 796. [CrossRef]
32. Oussaoui, S.; Boudhar, A.; Hadri, A.; Lebrini, Y.; Houmma, I.H.; Karaoui, I.; Kinnard, C. Mapping drought severity impact on arboriculture systems over Tadla and lower Tassaout plains in Morocco using Sentinel-2 data and machine learning approaches. *Geocarto Int.* **2025**, *40*, 2471104. [CrossRef]
33. Akhal, N. Les eaux souterraines au périmètre irrigué de Tadla entre le risque du réchauffement climatique et la demande en eau d'irrigation. *Espace Géogr. Soc. Maroc.* **2022**, *1*, 63.
34. El Mouine, Y.; El Hamdi, A.; Morarech, M.; Valles, V.; Yachou, H.; Dakak, H. Groundwater contamination due to landfill leachate: A case study of Tadla Plain. *Environ. Sci. Proc.* **2022**, *16*, 53. [CrossRef]
35. El Hamdi, A.; Morarech, M.; El Mouine, Y.; Rachid, A.; El Ghmari, A.; Yameogo, S.; Barbiero, L. Sources of spatial variability of soil salinity: The case of Beni Amir irrigated command areas in the Tadla Plain, Morocco. *Arid Land Res. Manag.* **2022**, *36*, 245–264. [CrossRef]
36. El Mouine, Y.; Rahoui, H.; El Hamdi, A.; Morarech, M.; Yachou, H.; Dakak, H. Assessment of groundwater quality for irrigation purposes in the Beni Moussa region, Tadla Plain, Morocco. *Ecol. Eng. Environ. Technol.* **2023**, *24*, 85–98. [CrossRef]
37. Badraoui, M.; Bellouti, A.; Lahlou, M.; Cherkaoui, F.-Z.; Chouraichi, M. Gestion de la salinité des sols et des eaux dans le périmètre irrigué du Tadla. In *Gestion Environmentale de L'Agriculture*; Actes Editions: Rabat, Morocco, 2005.
38. Parfonry, R.; Zaz, H.; Saaf, M. Analyse de systèmes de production au sein du périmètre irrigué du Tadla (Maroc). *Tropicultura* **1989**, *7*, 148–153.
39. Hammani, A.; Kuper, M.; Bekkar, Y.; Zaz, H. Exploitation des eaux souterraines dans le périmètre irrigué de Tadla (Maroc) Etat des lieux et éléments de méthodologie pour contribuer à une réflexion sur une gestion intégrée et durable des eaux souterraines et de surface. In Proceedings of the Economies d'eau en Systèmes IRrigués au Maghreb. Deuxième Atelier Régional du Projet Sirma, Marrakech, Morocco, 29–31 May 2006; Available online: https://hal.science/cirad-00272860/document (accessed on 30 June 2026).
40. Office Régional de Mise en Valeur Agricole du Tadla. Monographie. 2010. Available online: https://ormvasm.ma (accessed on 30 June 2026).
41. Hellegers, P.J.; Perry, C.J.; Petitguyot, T. Water pricing in Tadla, Morocco. In *Irrigation Water Pricing: The Gap Between Theory and Practice*; Molle, F., Berkoff, J., Eds.; CABI: Wallingford, UK, 2007; pp. 262–276.
42. Silatsa, F.B.; Kebede, F. A quarter century experience in soil salinity mapping and its contribution to sustainable soil management and food security in Morocco. *Geoderma Reg.* **2023**, *34*, e00695. [CrossRef]
43. Foster, T.; Mieno, T.; Brozović, N. Satellite-based monitoring of irrigation water use: Assessing measurement errors and their implications for agricultural water management policy. *Water Resour. Res.* **2020**, *56*, e2020WR028378. [CrossRef]
44. Peña-Arancibia, J.L.; Ahmad, M.U.D.; Yu, Y. Remote sensing characterisation of cropping systems and their water use to assess irrigation management from field to canal command scale. *Agric. Water Manag.* **2025**, *311*, 109374. [CrossRef]
45. Hochreiter, S.; Schmidhuber, J. Long short-term memory. *Neural Comput.* **1997**, *9*, 1735–1780. [CrossRef] [PubMed]
46. Hochreiter, S. The vanishing gradient problem during learning recurrent neural nets and problem solutions. *Int. J. Uncertain. Fuzziness Knowl. Based Syst.* **1998**, *6*, 107–116. [CrossRef]
47. Graves, A. *Supervised Sequence Labelling with Recurrent Neural Networks*; Springer: Berlin/Heidelberg, Germany, 2012.
48. Zhang, J.; Zhu, Y.; Zhang, X.; Ye, M.; Yang, J. Developing a Long Short-Term Memory based model for predicting water table depth in agricultural areas. *J. Hydrol.* **2018**, *561*, 918–929. [CrossRef]
49. Chang, Z.; Lu, W.; Wang, Z. Study on source identification and source-sink relationship of LNAPLs pollution in groundwater by the adaptive cyclic improved iterative process and Monte Carlo stochastic prediction. *J. Hydrol.* **2022**, *612*, 128109. [CrossRef]

50. Elzain, H.E.; Chung, S.Y.; Venkatramanan, S.; Selvam, S.; Ahemd, H.A.; Seo, Y.K. Novel machine learning algorithms to predict the groundwater vulnerability index to nitrate pollution at two levels of modeling. *Chemosphere* **2022**, *290*, 133217.
51. Yu, P.S.; Yang, T.C.; Kuo, C.C. Evaluating long-term trends in annual and seasonal precipitation in Taiwan. *Water Resour. Manag.* **2006**, *20*, 1007–1023. [CrossRef]
52. Guo, S.; Zhong, S.; Zhang, A. Privacy-preserving Kruskal-Wallis test. *Comput. Methods Programs Biomed.* **2013**, *112*, 135–145. [CrossRef] [PubMed]
53. MacFarland, T.W.; Yates, J.M. Kruskal-Wallis H-test for oneway analysis of variance by ranks. In *Introduction to Nonparametric Statistics for the Biological Sciences Using R*; Springer: Cham, Switzerland, 2016; pp. 177–211.
54. Palazón, L.; Navas, A. Variability in source sediment contributions by applying different statistic test for a Pyrenean catchment. *J. Environ. Manag.* **2017**, *194*, 42–53. [CrossRef]
55. Mouelhi, S.; Kanzari, S.; Ben Mariem, S.; Zemni, N. Towards a classification of Tunisian dams for enhanced water scarcity governance: Parametric or non-parametric approaches? *Hydrology* **2025**, *12*, 96. [CrossRef]
56. Pervez, M.S.; Brown, J.F. Mapping irrigated lands at 250-m scale by merging MODIS data and national agricultural statistics. *Remote Sens.* **2010**, *2*, 2388–2412. [CrossRef]
57. Said, H.; Nadia, E.; Hasan, O.; Mohamed, A. Assessment of land cover change impacts, 1987–2022, over environmental degradation using NDVI index and GIS tools within upstream part of Oum Err Bia Basin, Morocco. In *Technical and Technological Solutions Towards a Sustainable Society and Circular Economy*; Springer Nature: Cham, Switzerland, 2024; pp. 1–11.
58. Bekkar, Y.; Kuper, M.; Errahj, M.; Faysse, N.; Gafsi, M. On the difficulty of managing an invisible resource: Farmers' strategies and perceptions of groundwater use, field evidence from Morocco. *Irrig. Drain.* **2009**, *58*, S252–S263. [CrossRef]
59. Jamali, M.Y.; Namous, M. Impact of overexploitation of groundwater along the irrigated perimeter of Tadla, Oum Er-Rabia Basin, Morocco. *Desalin. Water Treat.* **2020**, *195*, 201–211. [CrossRef]
60. El Jamali, H. *Community-Based Water Management: The Oasis of Figuig, Morocco: Recent Extensions and Transformations*; Graduate Institute of International and Development Studies: Geneva, Switzerland, 2011.
61. Ouassanouan, Y.; Fakir, Y.; Simonneaux, V.; Hakim Kharrou, M.; Bouimouass, H.; Chehbouni, A. Sustainability issues of a Mediterranean semiarid irrigated piedmont inferred from multi-decadal trends of water resources and land use. In *EGU General Assembly Conference Abstracts*; EGU: Munich, Germany, 2022; p. EGU22-4725.
62. Capel, C. Contemporary oasis hydraulics: An open window on the sociology of the population of medieval Saharan cities. The case study of Sijilmasa, Morocco. *Afr. Débats Méthodes Terrains d'Hist.* **2023**, *14*. Available online: https://hal.science/hal-04517420/document (accessed on 30 June 2026). [CrossRef]
63. Houssni, M.; Kassout, J.; El Mahroussi, M.; Chakkour, S.; Kadiri, M.; Ater, M.; Petrisor, A.I. Evaluation and structuring of agrodiversity in oases agroecosystems of southern Morocco. *Agriculture* **2023**, *13*, 1413. [CrossRef]
64. El Baki, Y.; Boutoial, K.; Medaghri-Alaoui, A. Assessment of climate variability and agricultural activities in the area of Tadla Plain. *J. Geosci. Environ. Prot.* **2023**, *11*, 1–26. [CrossRef]
65. Hssaisoune, M.; Bouchaou, L.; Sifeddine, A.; Bouimetarhan, I.; Chehbouni, A. Moroccan groundwater resources and evolution with global climate changes. *Geosciences* **2020**, *10*, 81. [CrossRef]
66. Saak, A.E.; Peterson, J.M. Groundwater pumping by heterogeneous users. *Hydrogeol. J.* **2012**, *20*, 835–849. [CrossRef]
67. Kuper, M.; Hammani, A.; Chohin, A.; Garin, P.; Saaf, M. When groundwater takes over: Linking 40 years of agricultural and groundwater dynamics in a large-scale irrigation scheme in Morocco. *Irrig. Drain.* **2012**, *61*, 45–53. [CrossRef]
68. De Fraiture, C.; Giordano, M. Small private irrigation: A thriving but overlooked sector. *Agric. Water Manag.* **2014**, *131*, 167–174. [CrossRef]
69. Azemzi, H.; Erraoui, E.H. Irrigation water management and collective action: Understanding the shift from community management to participatory management in Souss-Massa, Morocco. *Euro-Mediterr. J. Environ. Integr.* **2021**, *6*, 1.
70. Labib, S.M.; Lindley, S.; Huck, J.J. Scale effects in remotely sensed greenspace metrics and how to mitigate them for environmental health exposure assessment. *Comput. Environ. Urban Syst.* **2020**, *82*, 101501. [CrossRef]
71. Gao, Y.; Huang, J.; Li, S.; Li, S. Spatial pattern of non-stationarity and scale-dependent relationships between NDVI and climatic factors: A case study in Qinghai-Tibet Plateau, China. *Ecol. Indic.* **2012**, *20*, 170–176. [CrossRef]
72. Xiong, Y.; Wang, H. Spatial relationships between NDVI and topographic factors at multiple scales in a watershed of the Minjiang River, China. *Ecol. Inform.* **2022**, *69*, 101616. [CrossRef]
73. Fan, J.; Fan, Y.; Cheng, J.; Wu, H.; Yan, Y.; Zheng, K.; Yang, Q. The spatio-temporal evolution characteristics of the vegetation NDVI in the Northern slope of the Tianshan mountains at different spatial scales. *Sustainability* **2023**, *15*, 6642. [CrossRef]
74. Priyan, K. Issues and challenges of groundwater and surface water management in semi-arid regions. In *Groundwater Resources Development and Planning in the Semi-Arid Region*; Springer: Cham, Switzerland, 2021; pp. 1–17.
75. Singh, K.; Jhorar, R.K.; Sidhpuria, M.S.; Kumar, M.; Mehla, M.K. Impacts of improved irrigation application efficiency and groundwater levels on energy use for crop production in a semi-arid region of India. *Environ. Dev. Sustain.* **2024**, *26*, 10145–10162.

76. Paswan, A.K.; Tiwari, V.M.; Agarwal, A.; Asoka, A.; Rangarajan, R.; Ahmed, S. Long-term spatiotemporal variation in groundwater recharge in the highly irrigated semi-arid region of India: The intertwined relationship between climate variability and anthropogenic activities. *Groundw. Sustain. Dev.* **2024**, *25*, 101145. [CrossRef]
77. Meza-Gastelum, M.A.; Campos-Gaytán, J.R.; Ramírez-Hernández, J.; Herrera-Oliva, C.S.; Villegas-León, J.J.; Núñez, A.F. Assessing groundwater dynamics and vegetation response in Ojos Negros Valley: A numerical simulation and NDVI study. *J. Hydrol.* **2025**, *647*, 133380. [CrossRef]
78. Wardlow, B.D.; Egbert, S.L. Large-area crop mapping using time-series MODIS 250 m NDVI data: An assessment for the US Central Great Plains. *Remote Sens. Environ.* **2008**, *112*, 1096–1116. [CrossRef]
79. Ouzemou, J.E.; El Harti, A.; Lhissou, R.; El Moujahid, A.; Bouch, N.; El Ouazzani, R.; El Ghmari, A. Crop type mapping from pansharpened Landsat 8 NDVI data: A case of a highly fragmented and intensive agricultural system. *Remote Sens. Appl. Soc. Environ.* **2018**, *11*, 94–103. [CrossRef]
80. Nhamo, L.; Ebrahim, G.Y.; Mabhaudhi, T.; Mpandeli, S.; Magombeyi, M.; Chitakira, M.; Sibanda, M. An assessment of groundwater use in irrigated agriculture using multi-spectral remote sensing. *Phys. Chem. Earth Parts A/B/C* **2020**, *115*, 102810. [CrossRef]
81. Bajocco, S.; Raparelli, E.; Teofili, T.; Bascietto, M.; Ricotta, C. Text mining in remotely sensed phenology studies: A review on research development, main topics, and emerging issues. *Remote Sens.* **2019**, *11*, 2751. [CrossRef]
82. Spadoni, G.L.; Cavalli, A.; Congedo, L.; Munafò, M. Analysis of normalized difference vegetation index multi-temporal series for the production of forest cartography. *Remote Sens. Appl. Soc. Environ.* **2020**, *20*, 100419. [CrossRef]
83. Robinson, N.P.; Allred, B.W.; Jones, M.O.; Moreno, A.; Kimball, J.S.; Naugle, D.E.; Richardson, A.D. A dynamic Landsat derived normalized difference vegetation index product for the conterminous United States. *Remote Sens.* **2017**, *9*, 863. [CrossRef]
84. Reynolds, R.W.; Rayner, N.A.; Smith, T.M.; Stokes, D.C.; Wang, W. An improved in situ and satellite SST analysis for climate. *J. Clim.* **2002**, *15*, 1609–1625. [CrossRef]
85. Chang, K.L.; Petropavlovskikh, I.; Cooper, O.R.; Schultz, M.G.; Wang, T. Regional trend analysis of surface ozone observations from monitoring networks in eastern North America, Europe and East Asia. *Elem. Sci. Anthr.* **2017**, *5*, 50. [CrossRef]
86. Cai, Z.; Jönsson, P.; Jin, H.; Eklundh, L. Performance of smoothing methods for reconstructing NDVI time-series and estimating vegetation phenology from MODIS data. *Remote Sens.* **2017**, *9*, 1271. [CrossRef]

Disclaimer/Publisher's Note: The statements, opinions and data contained in all publications are solely those of the individual author(s) and contributor(s) and not of MDPI and/or the editor(s). MDPI and/or the editor(s) disclaim responsibility for any injury to people or property resulting from any ideas, methods, instructions or products referred to in the content.